ORIGINAL ARTICLE

The Claustrum is Involved in Cognitive Processes Related to the Classical Conditioning of Eyelid Responses in Behaving Rabbits

M. Mar Reus-García[1], Raudel Sánchez-Campusano[1], Julia Ledderose[2,3], Godwin K. Dogbevia[3,4], Mario Treviño[3,5], Mazahir T. Hasan[3,6,7], Agnès Gruart[1] and José M. Delgado-García (iD)[1]

[1]Division of Neurosciences, Pablo de Olavide University, Seville 4103, Spain, [2]Institute of Biochemistry, Charité—Universitätsmedizin Berlin, Berlin 10117, Germany, [3]Max Planck Institute for Medical Research, Heidelberg 69120, Germany, [4]Division of Cardiac Surgery, University of Ottawa Heart Institute, Ottawa K1Y 4W7, Canada, [5]Laboratorio de Plasticidad Cortical y Aprendizaje Perceptual, Instituto de Neurociencias, Universidad de Guadalajara, Guadalajara 44130, México, [6]Laboratory of Memory Circuits, Achucarro Basque Center for Neuroscience, Leioa 48940, Spain, [7]Ikerbasque–Basque Foundation for Science, Bilbao 48013, Spain

Address correspondence to José M. Delgado-García, Division of Neurosciences, Pablo de Olavide University, Seville 41013, Spain. Email: jmdelgar@upo.es.

Abstract

It is assumed that the claustrum (CL) is involved in sensorimotor integration and cognitive processes. We recorded the firing activity of identified CL neurons during classical eyeblink conditioning in rabbits, using a delay paradigm in which a tone was presented as conditioned stimulus (CS), followed by a corneal air puff as unconditioned stimulus (US). Neurons were identified by their activation from motor (MC), cingulate (CC), and medial prefrontal (mPFC) cortices. CL neurons were rarely activated by single stimuli of any modality. In contrast, their firing was significantly modulated during the first sessions of paired CS/US presentations, but not in well-trained animals. Neuron firing rates did not correlate with the kinematics of conditioned responses (CRs). CL local field potentials (LFPs) changed their spectral power across learning and presented well-differentiated CL–mPFC/CL–MC network dynamics, as shown by crossfrequency spectral measurements. CL electrical stimulation did not evoke eyelid responses, even in trained animals. Silencing of synaptic transmission of CL neurons by the vINSIST method delayed the acquisition of CRs but did not affect their presentation rate. The CL plays an important role in the acquisition of associative learning, mostly in relation to the novelty of CS/US association, but not in the expression of CRs.

Key words: claustrum, classical eyeblink conditioning, local field potentials, rabbits, unitary recording, virus-delivered inducible silencing of synaptic transmission

Introduction

Since the original proposal of the claustrum (CL) as a structure involved in the integration of many different cortical and subcortical neural centers in order to generate conscious sensations (Crick 1994), we have seen a notable increase in the number of structural and hodological studies dealing with its peculiar central place in the brain and regarding its putative integrative role in higher brain functions. So far, the CL has been related to consciousness (Crick and Koch 2005; Kurada et al. 2019), salience detection (Smythies et al. 2012; Remedios et al. 2014; Smith et al. 2019), and segregation of attention (Mathur 2014; Goll et al. 2015; Atlan et al. 2018), among others topics. Although a number of reviews have also proposed a role of the CL in the integration of sensory information, perceptual binding, and internal functional states to generate cognitive-related processes (Edelstein and Denaro 2004; Crick and Koch 2005; Mathur 2014; Goll et al. 2015; Citri and Barretta 2016; Jackson et al. 2018), few studies address the contribution of CL neurons to associative learning, which certainly requires all the higher brain functions mentioned above.

The classical conditioning of eyelid responses is a well-known experimental procedure for the study of the neural basis of associative learning in mammals (Thompson 2005). It is generally assumed that the acquisition and storage of this type of learning takes place in the cerebellum (Krupa et al. 1993; Christian and Thompson 2003; Ten Brinke et al. 2017) or, at least, the timed performance of the acquired responses (Welsh and Harvey 1991; Sánchez-Campusano et al. 2007), mainly regarding delay paradigms. However, other brain structures also seem to participate in those processes. For example, motor cortices (MC) pyramidal neurons in rabbits fire well in advance of conditioned response (CR) initiation (Aou et al. 1992; Ammann et al. 2016). Moreover, electrical stimulation of the eyelid M1 area evoked motor responses with profiles and kinematics similar to those of CRs during classical conditioning (Ammann et al. 2016).

Still other cortical structures have been implicated in nonmotor, cognitive components of the acquisition, storage, and retrieval of eyelid CRs. For example, the hippocampus seems to be implicated in the acquisition of trace eyeblink conditioning paradigms, in which a silent gap separates conditioned stimulus (CS) and unconditioned stimulus (US) presentations (Berger et al. 1983; Thompson 2005). The activity of pyramidal hippocampal neurons is related to the salience of CS presentations across training and/or to the increasing CS/US associative strength (Rescorla 1988; Múnera et al. 2001), but not to the biomechanics of eyelid CRs, a coding property also ascribed to the rostral cingulate cortices (CC; Weible et al. 2003; Hattori et al. 2014). Likewise, specific areas of the medial prefrontal cotices (mPFC) have been proposed as participating in the proper determination of CS/US time intervals (Siegel and Mauk 2013; Caro-Martín et al. 2015) and in partial reinforcement (Powell et al. 2005). The mPFC also plays a permissive role in the initial release of eyelid CRs, because its electrical stimulation in behaving rabbits prevents the expression of CRs, but CR acquisition (Leal-Campanario et al. 2007, 2013).

The CL is the most interconnected region per volume in the brain (Torgerson et al. 2015). Given its dense reciprocal connections with the above-mentioned cortical structures described above, CL neurons could also play an important role in motor and/or nonmotor neural activities related to classical eyeblink conditioning. Furthermore, it has been reported that CL neurons respond to numerous sensory stimuli (Spector et al. 1974; Olson and Graybiel 1980; Sherk and LeVay 1981; Remedios et al. 2010), a crucial requirement for this kind of associative learning.

Different experimental laboratory species, ranging from humans to mice, have been used in the study of this thin and irregular structure. Rodents are commonly used despite the fact that they present small CLs, not very well-separated from cortex (Binks et al. 2019). Consequently, targeting the CL may be complicated, and single-unit recordings are difficult to attain when animals are awake. Because CL volume increases with the cerebral hemisphere volume (Kowiański et al. 1999), the CL of rabbits and guinea pigs offers interesting possibilities given its size and isolated location. Compared with that of mice, the rabbit CL is a prominent structure, seven times larger in volume than the CL of mice. Further, the rabbit CL is distinctly separated from surrounding structures (i.e., the insular cortex and the putamen) by the fibers of a well-developed external and extreme capsule (Girgis and Shih-Chang 1981; Kowiański et al. 1999). These advantages facilitate targeting the CL during the in vivo recordings performed here. In addition, although CL volume and shape vary across species, a vast connectivity with the cortex seems to be a well-conserved characteristic of the CL in monkeys (Druga et al. 1990), cats (Druga 1982), mice (Atlan et al. 2017), rats (Majak et al. 2000), and rabbits (Kowiański et al. 1997, 2000).

For all the above reason, rabbits were prepared for recording the unitary activity of CL neurons during classical eyeblink conditioning, using a delay paradigm since CL is a pallial subcortical structure (Binks et al. 2019). In fact, trace conditioning is preferentially related to cortical structures (Clark et al. 1984; Takehara-Nishiuchi et al. 2005; Gruart et al. 2006; Oswald et al. 2009).

Previous research has established that the integral of the rectified electromyographic (EMG) activity of the orbicularis oculi (O.O.) muscle can precisely determine eyelid position (Gruart et al. 1995; Schade Powers et al. 2010). Therefore, implanting a recording electrode in the O.O. muscle, we could ascertain whether animals closed the eye due to CS presentations (i.e., as a CR), or to US presentations (i.e., as a UR), and monitor the learning process (Gruart et al. 2000; Leal-Campanario et al. 2007). Recorded CL neurons were classified according to their firing profiles during paired CS/US presentations. Their firing rates were found to be related to the acquisition process but not to the changes in latency and strength presented by CRs across training. Local field potentials (LFPs) recorded in CL, MC, and mPFC changed their spectral powers across conditioning sessions for all the selected frequency bands. Significant delta–gamma comodulations were detected at CL–mPFC network nodes during certain conditioning phases. Finally, the inactivation of CL neuron synaptic connectivity affected the number but not the amplitude of CRs. In accordance, the CL seems to be directly involved in cognitive aspects of the process of acquiring eyelid CRs, such as attention to CS salience (Múnera et al. 2001; Atlan et al. 2018), but not in their proper performance (Ammann et al. 2016).

Material and Methods

Experimental Animals

Experiments were carried out in male rabbits (New Zealand white albino) obtained from an authorized supplier (Isoquimen, Barcelona, Spain). Animals were 2.5–3-months old and weighing

2–2.4 kg on arrival at the Animal House facilities of Pablo de Olavide University (Seville, Spain). Upon their arrival, animals were housed in individual cages provided with a burrow and different environmental stimuli, where they were maintained for the whole experiment. The room was kept on a 12/12 h light/-dark cycle with constant ambient temperature (21 ± 1 °C) and humidity (55 ± 7%). Food and water were available ad libitum.

Experiments were carried out following European Union Council (2010/276:33–79/EU) guidelines and Spanish (BOE 34:11370-421, 2013) regulations for the use of laboratory animals in chronic experiments. Experiments were also approved by the local Ethics Committee of Pablo de Olavide University.

Surgery

Animals were anesthetized with an intramuscular injection of a ketamine–xylazine cocktail (Ketaminol, 50 mg/mL; Rompun, 20 mg/mL; and atropine sulfate, 0.5 mg/mL) at an initial dosage of 1.0 mL/kg. Anesthesia was maintained by intravenous perfusion (93% saline, 4% Ketaminol, and 3% Rompun) at a flow rate of 10 mL/kg/h.

A first group of animals ($n = 7$) were prepared for the chronic recording of unitary activity in the CL during classical eyeblink conditioning ($n = 5$) and pseudoconditioning ($n = 2$) (Figs 1A–D and 2–4). A window (2 × 5 mm) was drilled through the parietal bone centered overlying the right rostral CL (rostral corners from bregma: AP = 4 mm, L = −4 to −6 mm; caudal corners: AP = −1 mm, L = −7.5 to −9.5 mm; Girgis and Shih-Chang 1981). A recording chamber was built with acrylic cement around the window and a sterile pin was fixed to one anterolateral corner of the recording window for reference purposes. The dura mater was removed, and the cortical surface was protected with an inert plastic cover and sterile gauze between recording sessions. A silver electrode (1 mm in diameter) was attached with small screws to the right bone as a ground. All these animals were implanted bilaterally with stimulating electrodes in the M1 subdivision of the MC (AP = 2 mm, L = +2 mm and −2 mm; D = 1.5 mm, with respect to brain surface; Girgis and Shih-Chang 1981) corresponding to the eyelid motor area (Ammann et al. 2016). In addition, five of them were also implanted with electrodes aimed at the prelimbic area of the mPFC (AP = 11 mm, L = +1 mm and −1 mm; D = 2.5 mm; Girgis and Shih-Chang 1981), while the other two were implanted in the CC (AP = 4 and 0 mm, L = +2 and −2 mm; D = 1.5 mm)—namely, three areas related with classical eyeblink conditioning (Weible et al. 2003; Caro-Martín et al. 2015; Ammann et al. 2016) and projecting to the CL (Smith and Alloway 2010; Atlan et al. 2017; White et al. 2017; Jackson et al. 2018). Stimulating electrodes were made with 200 μm varnished silver wire (California Fine Wire Company, CA, USA) bared ≈0.5 mm at the tip. Finally, animals were implanted with bipolar hook electrodes in both O.O. muscles to record their EMG activity (Fig. 2A). These electrodes were handmade from multistranded Teflon-coated stainless-steel wire (A-M Systems) with a total external diameter of ≈0.2 mm and bared ≈0.5 mm at the tip. For head-holding fixation during unitary recordings, animals were implanted with a head-holding device, made from three bolts cemented to the skull perpendicular to the stereotaxic plane. Stimulating and recording electrodes were connected to two nine-pin sockets affixed to the holding system.

A second group of animals ($n = 4$) were prepared for the chronic recording of LFPs in CL, MC, and mPFC (Figs 5 and 6 and Supplementary Fig. 1A,B,D). For this experiment, animals were implanted bilaterally with recording tetrodes in the rostrodorsal part of the CL (AP = 1 mm, L = +6.5 and −6.5 mm; D = 6.5 mm; Girgis and Shih-Chang 1981) and with recording bipolar electrodes in the mPFC (AP = 11 mm, L = +1 and −1 mm; D = 2.5 mm; Girgis and Shih-Chang 1981) and in the MC (AP = 2 mm, L = +2 and −2 mm; D = 1.5 mm; Girgis and Shih-Chang 1981). These electrodes were handmade from two (bipolar) or four (tetrodes) threads of 50 μm, Teflon-coated tungsten wire (Advent Research Materials Ltd). Animals were also implanted bilaterally with recording EMG electrodes in both upper eyelids and with a ground wire. All wires were soldered to three nine-pin connectors. Finally, animals were implanted with a head-holding system as described above.

A third group of animals ($n = 8$) were infected with a mix of recombinant adeno-associated viruses (rAAVs) equipped with enhanced green fluorescent protein (EGFP) and doxycycline-dependent tetracycline-controlled genetic switches, which release tetanus toxin (TeTxLC) and tandem dimer Tomato (tdTOM) when activated (vINSIST method, see below and Supplementary Appendix 1) (Fig. 7). These animals received a total of three microinjections (each of 2 μL) of the viral suspension in each CL (rostral, AP = 4 mm, L = +5 and −5 mm; D = 5 mm; medial, AP = 2 mm, L = +7 and −7 mm; D = 5.5 mm; and caudal, AP = 0.5 mm, L = +8 and −8 mm; D = 6 mm; Girgis and Shih-Chang 1981). Injections were carried out in both CLs, since it has been described as a powerful functional compensation system (Duffau et al. 2007). A 5 μL microsyringe (Hamilton®) was used for injecting the rAAVs. These animals were also implanted bilaterally with recording EMG electrodes in both upper eyelids and with a ground wire. All wires were soldered to one nine-pin connector. Finally, animals were implanted with a head-holding system as described above.

Recording and Stimulating Procedures

The initial training of the animals was started 1 week after surgery and lasted for 5 days. We used a Perspex box designed to limit the animal's movements (Gruart et al. 2000; Leal-Campanario et al. 2007). The box was placed on the recording table. The recording room was kept softly illuminated and the recording table was surrounded by a black cloth. The first two recording sessions were aimed at adapting the animal to the recording conditions. No stimulus was presented during these two sessions.

The EMG activity of the O.O. muscle and LFPs were recorded using Grass P511 differential amplifiers with a bandwidth of 0.1 Hz to 10 kHz (Grass-Telefactor).

Unitary recordings from CL neurons were carried out with glass micropipettes filled with 2 M NaCl (3–5 MΩ of resistance) and filtered analogically in a bandwidth of 1 Hz to 10 kHz (AC/DC differential amplifier; model 3000, A-M Systems). On occasion, we used tungsten microelectrodes of 5 MΩ of resistance (A-M Systems) for unitary recordings and local microlesions. The recording area was approached with the help of stereotaxic coordinates (Girgis and Shih-Chang 1981), and antidromic or orthodromic field and unitary potentials were evoked by electrical stimulation of MC, CC, and/or mPFC. To determine whether the recorded and the activated neuron were the same, we used the collision test (i.e., the antidromic invasion of a soma is prevented if the antidromic action potential collides with a spontaneous orthodromic action potential; see Fig. 1G1, and Múnera et al. 2001; Ammann et al. 2016). At the end of each recording session,
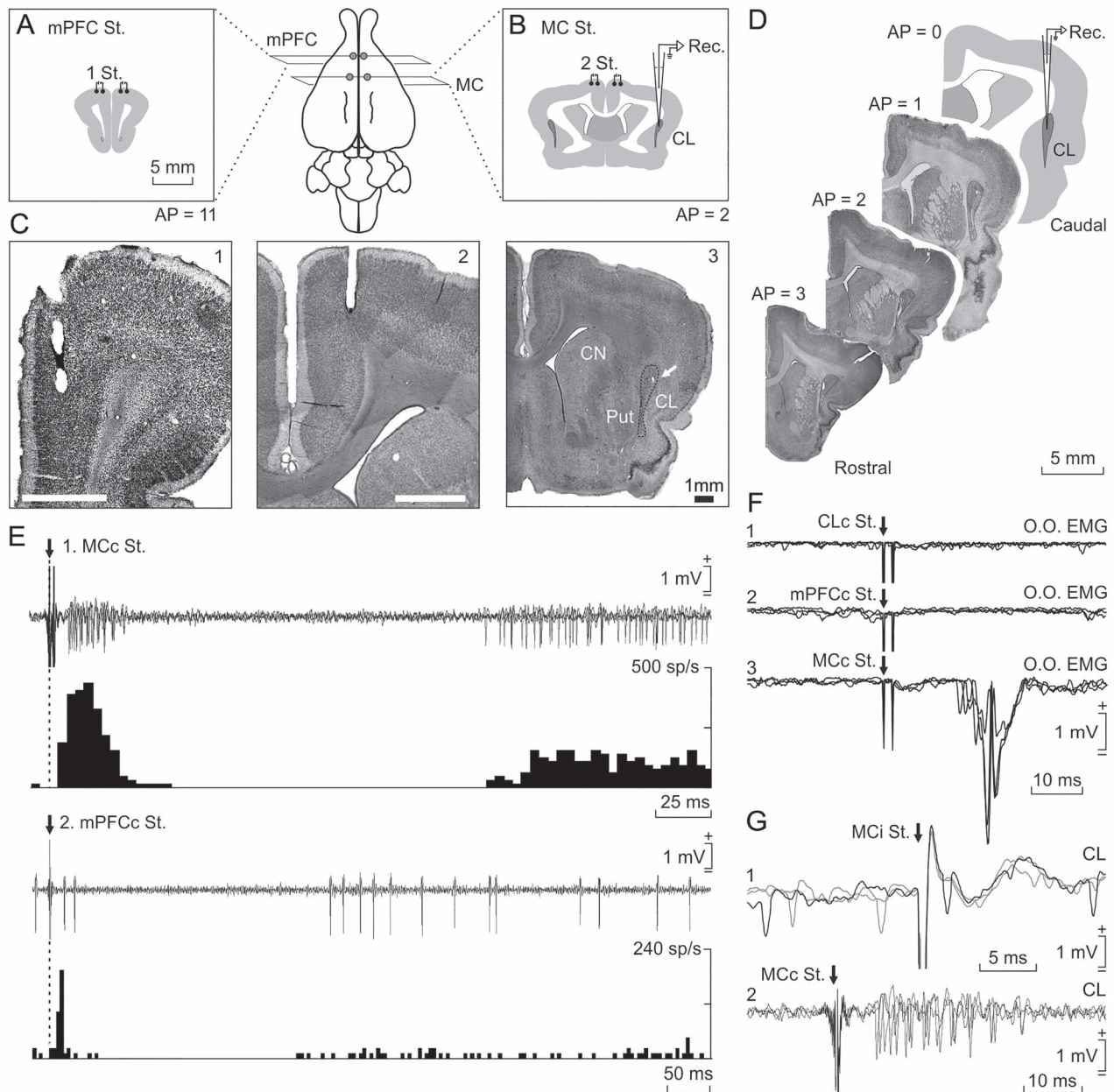
Figure 1. Location and identification of recorded neurons. Rabbits were bilaterally implanted with chronic stimulating electrodes in mPFC (A), M1 subdivision of MC (B), and CC (not illustrated). (C) Photomicrographs of coronal sections illustrating the location of stimulating electrodes in mPFC (1) and M1 (2). In (3), a microlesion in the dorsal CL is illustrated (arrow); it was carried out with a metal electrode implanted in a selected recording area; CN, caudate nucleus; Put, putamen. (D) Diagram of recording sites and images from targeted CL in four anteroposterior sections. The activity of CL neurons was recorded with glass micropipettes from rostral and central parts of the right dorsal CL (dotted line). Drawings in A, B, and D follow the atlas of Girgis and Shih-Chang (1981). (E) Three overlapped recordings illustrating short- and long-term synaptic activation of a CL neuron activated from the contralateral MC (1) and another one activated from the contralateral mPFC (2). Below each one is illustrated the peristimulus time histogram of 15 recordings. (F) From top to bottom are illustrated the EMG activity evoked in the left O.O. muscle by double pulses (2 ms interval) applied to the contralateral CL (1), mPFC (2), and MC (3). (G) Three overlapped recordings illustrating a CL neuron antidromically activated from the ipsilateral MC during the spike-triggered collision test (1). (2) illustrates the synaptic activation of a representative CL neuron from the contralateral MC.

the recording chamber was sterilized and closed with an inert plastic cover and sterile gauze and covered with bone wax.

Electrical stimulation of electrode-implanted sites consisted of single (square, 50 μs, 0.1–0.5 mA, positive–negative pulses with 20 μs of interval) or paired (1–2 ms of interval) pulses programmed with a CS-20 stimulator across an ISU-200-BIP isolation unit (Cibertec).

Classical Eyeblink Conditioning

Eyeblink conditioning was achieved using a delay conditioning paradigm (see Fig. 2 and Leal-Campanario et al. 2007). A 350-ms tone (600 Hz, 90 dB) was presented as CS and a 100-ms air puff (3 kg/cm^2) directed at the left cornea was used as US. The US was prepared to coterminate with the CS. The concept
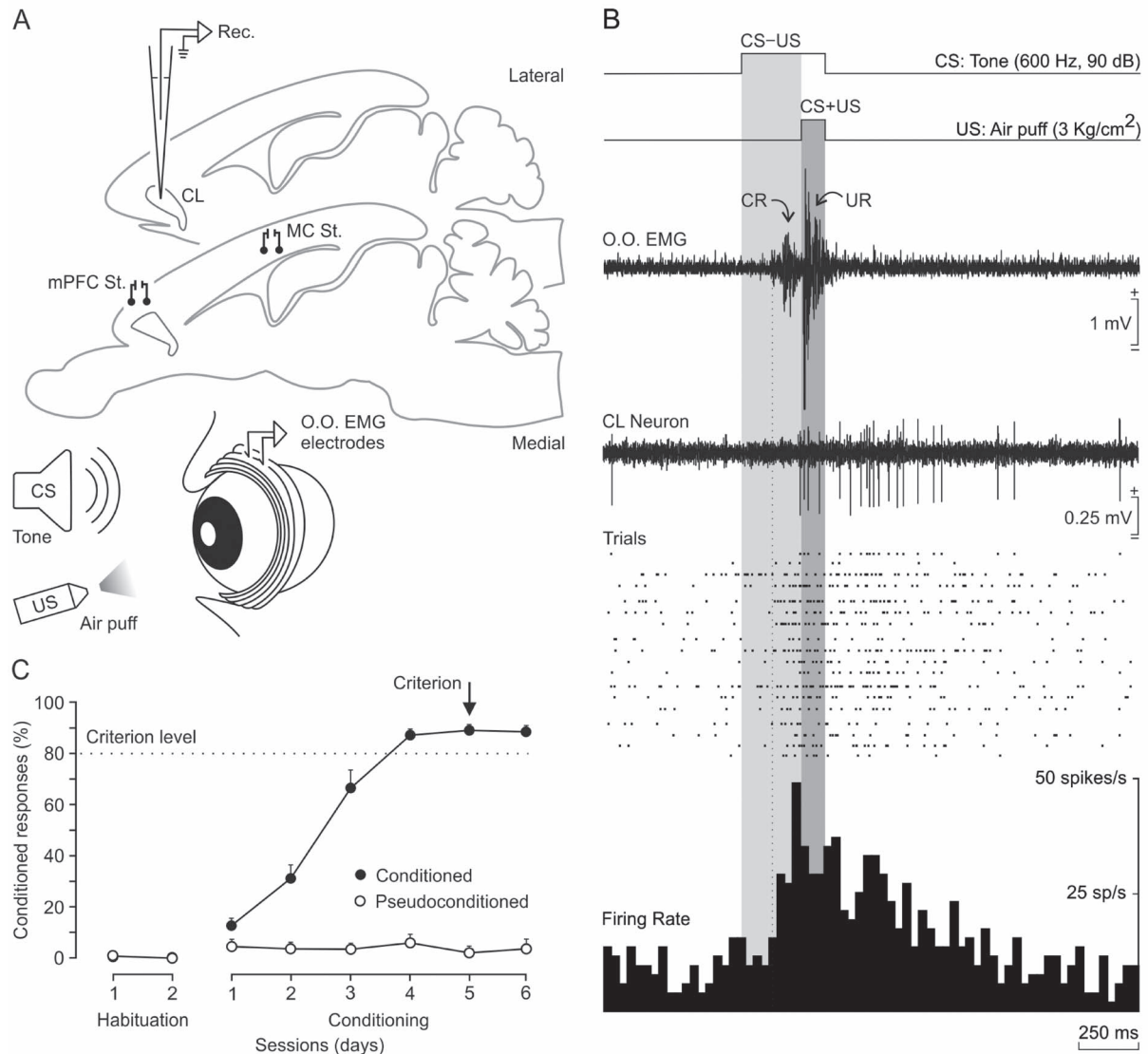
Figure 2. Classical eyeblink conditioning using a delay paradigm. (A) In addition to the stimulating electrodes, rabbits were implanted with EMG recording electrodes in the left O.O. muscle (O.O. EMG) aimed at recording CRs. (B) Representation of the delay paradigm and the firing activity of a selected CL neuron recorded during the fifth conditioning session. From top to bottom are shown: (1) the CS (a tone; 600 Hz, 90 dB, 350 ms); (2) the US (a corneal air puff; 3 kg/cm^2, 100 ms); (3) one example of the EMG activity of the O.O. muscle—note the presence of the CR in the CS–US interval as a learning-dependent response (light gray area) and the UR in the CS + US period as a reflex reaction (in dark gray area)—(4) the firing activity of a CL neuron during a CS/US presentation; (5) a raster plot of 18 successive CS/US trials; and (6) the peristimulus time histogram of all of them (in spikes/s). (C) Evolution of the percentage of CRs across six conditioning sessions for five conditioned and two pseudoconditioned rabbits. Note that conditioned animals reached the selected criterion (≥80% of CRs for two consecutive days) by the fifth conditioning session.

"CS/US" refers solely to the presentation of the pair of stimuli. We term "CS–US" the first 250 ms of the CS, right before the start of the US. It is during this time frame that CRs are expected to be found throughout conditioning. We considered a "CR" the presence, during the CS–US period, of the EMG activity of the left O.O. muscle lasting >10 ms and initiated >50 ms after CS onset (Gruart et al. 2000). We use "CS + US" to refer to this 100 ms coexisting period; UR will appear during this period. Recordings from the right O.O. muscle were used as a control for spontaneous and/or voluntary eyelid movements.

A function generator (AFG 3022B, Tektronix), triggered by a digital programmer (3.2-Microstim, Cibertec), was used to generate the train with tone characteristics (600 Hz, sine wave, 1 V). An amplifier (PA Amplifier FS-2035, Fonestar Systems, Madrid,

Spain) converted the pulse to a tone (90 dB) via a loudspeaker located 60 cm in front of the animal. Air puffs were delivered from an air compressor (Biomedical Engineering) and applied through the opening of a plastic pipette (3 mm in diameter) attached to the animal's holding system and located 1 cm from the left cornea.

The first two sessions were aimed at adapting the animal to the experimental conditions. No stimulus was presented during these two sessions. Following them, unless otherwise indicated, animals received two habituation sessions (during which the CS was presented alone) and eight conditioning sessions (paired CS/US) (n = 5 rabbits). Both habituation and conditioning sessions consisted of 66 trials (6 series of 11 trials each). Successive trials were separated at random by intervals of 45–60 s
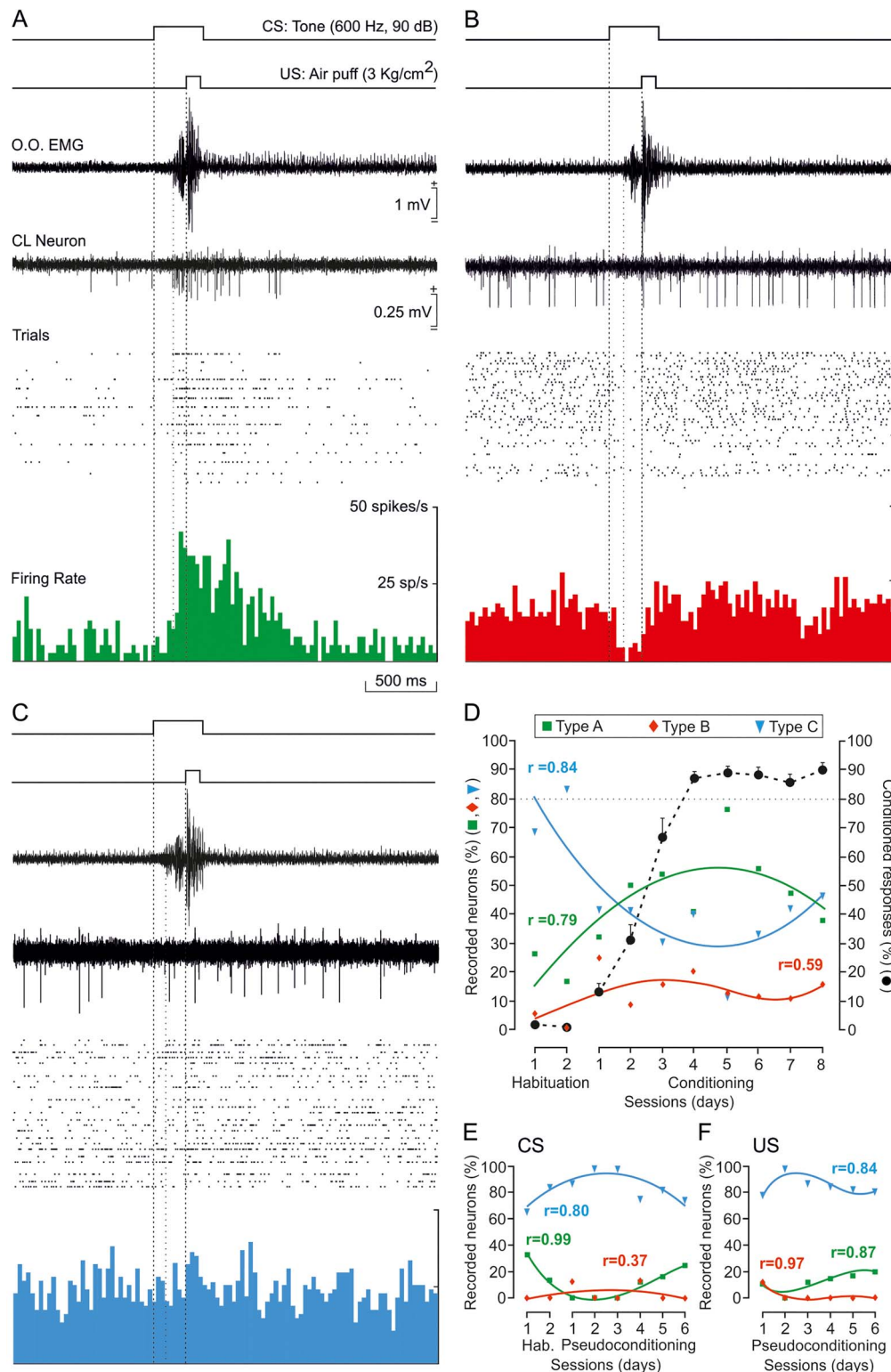
Figure 3. Types of firing rate recorded from CL neurons during classical eyeblink conditioning. (A) Example of a type A neuron, activated in advance of US onset, and recorded during the fifth conditioning session. (B) Example of a type B neuron, inhibited well in advance of the beginning of the CR, and recorded during the eighth conditioning session. (C) Example of a type C neuron, unrelated to the classical conditioning task, and recorded during the third conditioning session. Traces illustrated from top to bottom as in Figure 2B. Calibrations in A are also for B and C. (D) Percentages of claustral neurons ($n = 130$ from $n = 5$ rabbits) activated (green squares and lines), inhibited (red diamonds and lines), or unrelated (blue triangles and lines) to habituation and eight conditioning sessions. The black dotted line indicates the learning curve. (E,F) Percentages of CL neurons activated, inhibited, and unrelated to CS ($n = 47$ from $n = 2$ rabbits; E) or US ($n = 40$ from $n = 2$ rabbits; F) presentations during habituation and six pseudoconditioning sessions. Collected neuronal data in D–F were best represented with quadratic or higher order polynomial fits (see Supplementary Table 3). The regression coefficients (r) for the illustrated polynomial fits are indicated. The statistical performance was calculated according to the confidence interval (95%, $P < 0.05$).
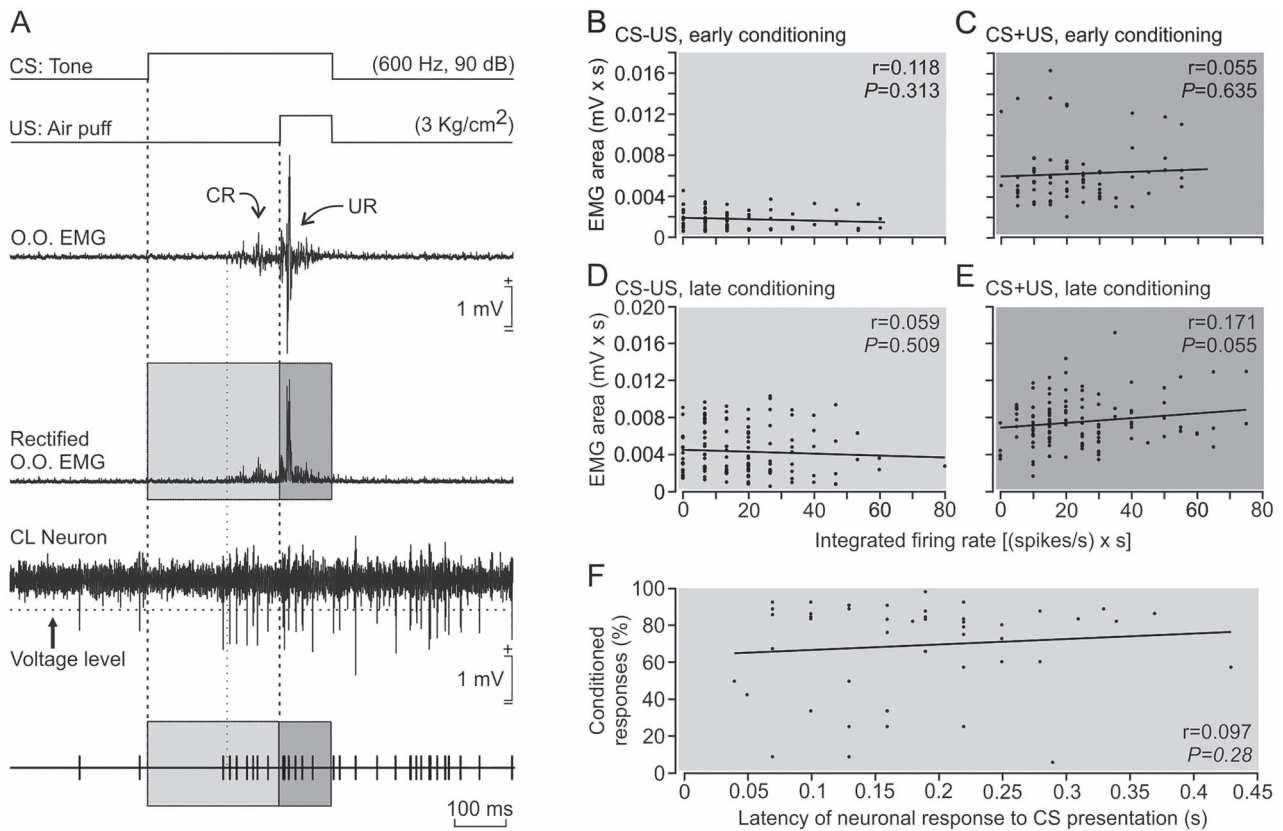
Figure 4. Relationships between changes in the firing rate of type A neurons and the EMG activity of the O.O. muscle and the percentage of CRs across conditioning. (A) From top to bottom are shown: a representation of the conditioning stimuli, one example of the EMG activity of the O.O. muscle with its rectified version below, the firing activity of a type A CL neuron during a CS/US presentation, and a representation of action potentials reaching the selected voltage level. For these analyses, we quantified the EMG area (mV × s) versus the integrated firing frequency [in (spikes/s) × s] during the CS–US period (light gray area) and also during CS + US interval (dark gray area)] ($n = 5$ rabbits). (B,C) Linear relationships between the EMG area and the integrated firing frequency of type A neurons for the CS–US interval (B) and the CS + US period (C) during early (first to third) conditioning sessions ($n = 75$ trials from $n = 17$ neurons). (D,E) Same relationships as in B and C but during late (fourth to eighth) conditioning sessions ($n = 127$ trials from $n = 25$ neurons). (F) Relationship between the activation latency of type A neurons after CS presentations and the percentage of CRs ($n = 51$ neurons). Note the low values of regression coefficients (r) for all the illustrated relationships (see Supplementary Table 5).

(3.2-Microstim, Cibertec). During conditioning sessions, the first trial of each one of the six series consisted of a test trial in which the CS was presented alone (a total of six test trials per session). As selected criterion for learning, the animals had to generate ≥80% of CRs in two successive conditioning sessions. Pseudoconditioned animals ($n = 2$ rabbits) received two habituation sessions as described above and six pseudoconditioning sessions (all conditioned animals learned the task and reached the criterion before the sixth conditioning session) with unpaired, randomized CS and US presentations. All sessions lasted ~80 min. Unitary and/or field recordings were carried out during all of the indicated sessions.

Histology

Once the electrophysiological experiments were finished, animals were deeply anesthetized with sodium pentobarbital (50 mg/kg, i.p.), and perfused transcardially with saline and 4% paraformaldehyde. The proper location of eyelid EMG and stimulating electrodes was checked. To facilitate the location of recording sites in the CL, a small electrolytic lesion (0.2–0–4 mA of anodic current for 30 s; CS-220 stimulator across an ISU-200-BIP isolation unit; Cibertec) was carried out during the final

recording sessions and relevant coronal sections were processed for Nissl staining. Recording sites were adjusted according to the collected stereotaxic coordinates and with the location of the electrolytic marks (Fig. 1C,D and Supplementary Fig. 1D).

The vINSIST Method

We developed an advanced method for doxycycline (Dox)-controlled virus-delivered inducible silencing of synaptic transmission (vINSIST) between connected circuits. The three rAAVs contained in the injected mix were as follows: (1) rAAV–PhSYN–rtTA, (2) rAAV–Ptetbi–TeTxLC/tdTOM, and (3) rAAV–PhSYN–EGFP. We engineered the tetanus toxin light-chain coding sequence (TeTxLC) for selective cleavage of synaptobrevin-2 (Syb-2) to block synaptic transmission (Sweeney et al. 1995) into a bidirectional tetracycline promoter (P_{tet}bi) (Hasan et al. 2013; Dogbevia et al. 2015, 2016) with TeTxLC on one side and tandem dimer Tomato gene (tdTOM, expressing red fluorescent protein) on the other (rAAV–Ptetbi–TeTxLC/tdTOM). A reverse tetracycline transactivator (rtTA) and EGFP are independently expressed under the human synapsin promoter (rAAV–PhSYN–rtTA and rAAV–PhSYN–EGFP), so rtTA-infected cells will be traceable in green. With the addition of Dox, a hydrophobic
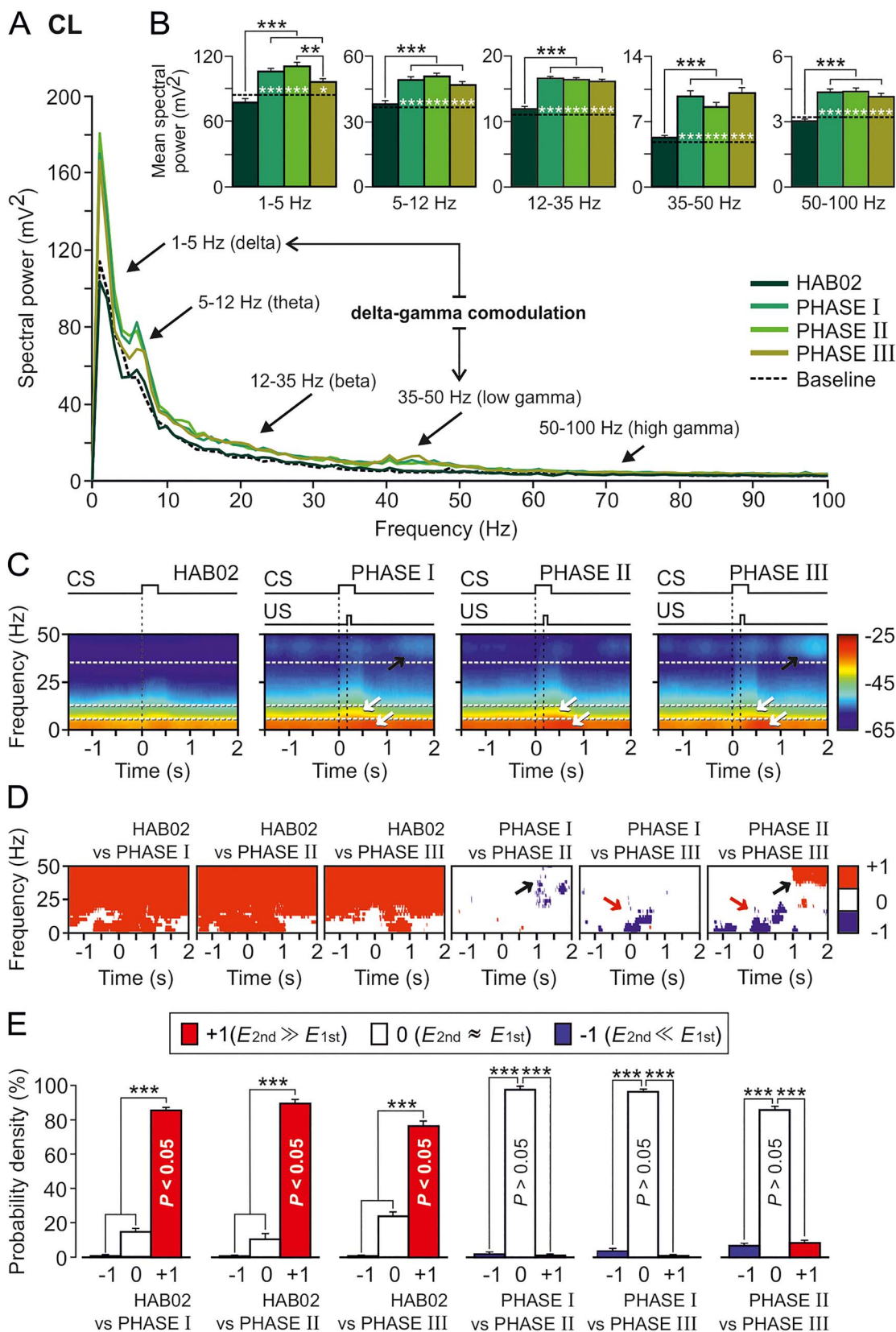
Figure 5. Spectral analyses of LFPs recorded in the CL during classical eyeblink conditioning. LFPs were recorded during habituation and conditioning phases from four rabbits. (A) Mean power spectra of LFPs recorded in the CL for 120 3.5 s frames (between 1.5 s before and 2 s after CS presentation) for four of the conditions (HAB02, phase I, phase II, and phase III) and for 3.5 s baseline frames (taken from HAB02 sessions but including no stimulus). The black arrows indicate the spectral ranges

derivative of tet that rapidly crosses the blood–brain–barrier, rtTA binds P_{tet}bi and activates the expression of TeTxLC (to silence synaptic transmission) and tdTOM (thus the inhibited location will glow in red; Fig. 7 and Supplementary Fig. 2 and Supplementary Appendix 1).

Rabbit Brain Slices

Brains from the vINSIST-injected rabbits were fixed in PFA (4%) at 4 °C overnight. Brains were then cut by a vibratome (Leica VT 1000S) in sections 140 μm thick. The sections were mounted in glycerol (80% in PBS + 2.5% DAPCO). Slices were imaged on a confocal laser scanning microscope (Leica TCS SP5) using a 10× air objective and a 20× oil immersion objective and a 488 nm argon laser. Images were taken in z-stacks of 2 and 3 μm on the 10× and the 20× objectives, respectively.

Data Collection and Analysis

The unrectified EMG activity of the O.O. muscle, the unitary activity of CL neurons, LFPs recorded in the CL, and 1-volt rectangular pulses corresponding to CS and US presentations were acquired online through an 8-channel analog-to-digital converter (CED 1401-plus, CED, Cambridge, UK), and transferred to a computer for quantitative offline analysis. Data were sampled at 4 kHz for LFP recordings, 5 kHz for EMG activities, and 25 kHz for unitary recordings, with an amplitude resolution of 12 bits.

Computer programs (Spike2 and SIGAVG from CED) were used to display unrectified and rectified EMG, unitary activities, and LFPs (Figs 2–6 and Supplementary Fig. 1). As illustrated in Figures 1–4, the recorded neuron was generally easy to identify. In the case of multiple unitary recordings in which it was difficult to identify a single cell, a spike sorting (from Spike2, CED) was carried out. In all cases, an event channel was created for each identified neuron in which each event corresponded to a single spike. The representation programs enabled display of event rasters of unitary activities and the poststimulus time histograms (PSTHs). Following Rieke et al. (1997), PSTHs were converted to firing rates as a function of time (i.e., in spikes/s) for the characterization of the firing properties of the CL neurons. For the classification of the CL neurons in different groups, we used not only their firing rate profiles but also spike duration parameters (see Supplementary Fig. 3 and Supplementary Appendix 2).

Programs also enabled quantifying the activation latencies of CRs (ms) and unitary recordings (ms), the rectified EMG areas (mV × s or mV × ms), and the integrated firing rate [(spikes/s) × s] (Caro-Martín et al. 2015; Ammann et al. 2016).

Statistical analyses for unitary and EMG activities were carried out using the Sigma Plot 11.0 package (Sigma Plot) and the Statistics MATLAB Toolbox (version 9.4, R2018a; The MathWorks) for Windows, for a statistical significance level of $P < 0.05$. Mean values are followed when necessary by their standard error mean (SEM). Statistical differences of mean values were determined by analysis of variance (ANOVA). Regression analyses were carried out using ≥ 50 measurements collected from at least four animals.

From spectral analyses, we selected LFP epochs lasting 3.5 s (1.5 s preceding and 2 s following CS presentation). Analyses in the frequency domain were carried out in accordance with the following frequency bands: delta (1–5 Hz), theta (5–12 Hz), beta (12–35 Hz), low gamma (35–50 Hz), and high gamma (50–100 Hz). The processing of LFP recordings both in the frequency domain by means of fast Fourier transforms (FFT; Figs 5A and 6A,D,G,J) and in the time–frequency domain by means of multitaper Fourier transforms (mTFT; Figs 5C and 6C,F,I,L) were carried out using homemade programs (Jurado-Parras et al. 2013; Fernández-Lamo et al. 2016) written in the MATLAB platform (version 9.4, R2018a; The MathWorks) and customized scripts of Chronux (Mitra and Bokil 2008; Bokil et al. 2010) software (versions 2.11/R2014 and 2.12/R2018. Website: http://chronux.org/). Probability maps for the comparison of pairs of spectrograms were generated following previous descriptions by our group (Fernández-Lamo et al. 2016). In addition, to assess the putative spectral couplings between different oscillatory activities from LFP recordings, the crossfrequency correlation (Masimore et al. 2004) as a measure of comodulation and the power–power spectral ratios were calculated (see Supplementary Appendix 3).

For multivariate statistics assessments, both parametric (Fisher ANOVA F-tests, without or with repeated measures) and nonparametric [ANOVA tests on ranks, without repeated measures (Kruskal–Wallis ANOVA)] methods were used to assess the statistical significance of differences between groups, followed by the appropriate test (Holm–Sidak, Tukey–Kramer, or Student–Newman–Keuls tests, in this order of priority when the group sizes are equal; and the Dunn's test when the sizes are different) for all the pairwise multiple-comparison analyses (Jurado-Parras et al. 2013; Fernández-Lamo et al. 2016).

---

corresponding to delta (1–5 Hz), theta (5–12 Hz), beta (12–35 Hz), and low- (35–50 Hz) and high- (50–100 Hz) gamma bands. Although the fundamental contribution to CL power spectrum was determined by delta and theta frequency bands, prominent (well-differentiated) power peaks appeared in delta and low gamma bands during phases I and III. Therefore, the resulting delta–gamma comodulation is also indicated. (B) Histograms of mean spectral powers for all the defined frequency bands. Note that the start of conditioning phases significantly increased the spectral powers in the five frequency bands (Tukey–Kramer multiple comparison test: HAB02 and Baseline vs. phases I, II, and III; ***$P < 0.001$). Also note that baseline values (dotted black line) were very similar to those collected during the presentation of the unpaired CS (HAB02). (C) Time–frequency representations (spectrograms; $N_T \times K = 600$ tapered Fourier transforms) corresponding to data from HAB02 and conditioning phases I, II, and III illustrated in A and B. Note that maximum spectral powers (see the color calibration bar at the right) for delta and theta occurred during and shortly after CS/US presentations, in the three conditioning phases (white arrows), but maxima for low gamma appeared 1 s after the CS/US, during phases I and III (black arrows). (D) Multiple comparisons between the different spectrograms and their corresponding probabilistic maps according to the jackknifed variance criterion. Red (inference type +1; power in first spectrogram ≫ power in second spectrogram) and blue (inference type −1; power in first spectrogram ≪ power in second spectrogram) indicate significant statistical differences ($P < 0.05$; jackknifed estimates of the variance), and white (inference type 0; power in first spectrogram ≈ power in second spectrogram) indicates no significant differences ($P > 0.05$). Black arrows indicate that the spectral powers in the low-gamma frequency band were higher in phases I and (especially) III when comparing with phase II; that increment occurred at the end (range between 1 and 2 s after the CS/US presentation) of the analyzed epoch. Red arrows show how, in contrast, spectral powers in low frequencies were higher in phases I and (especially) II when comparing with phase III during and slightly after the CS/US presentation. (E) Histograms of mean probability densities. Here, it is very evident (***$P < 0.001$, Tukey–Kramer test) that there are statistically significant differences ($P < 0.05$, red bars) between the habituation (HAB02) and the conditioning (I, II, and III) phases in practically the whole time–frequency range. Although they present some specific significant differences in delta, theta, and low gamma bands, the three conditioning sessions are not statistically different overall ($P > 0.05$, white bars).
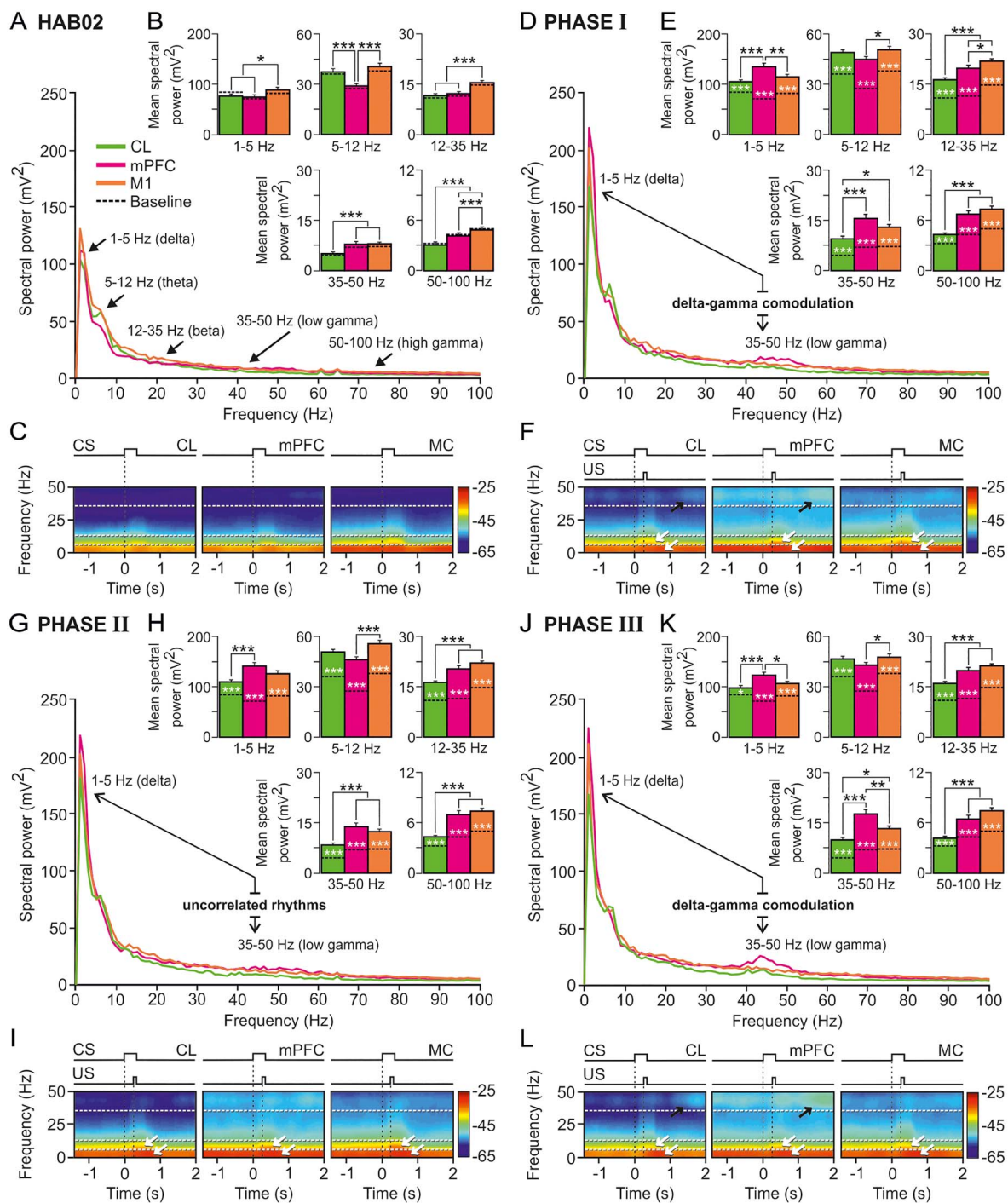
Figure 6. Spectral analyses of LFPs recorded in CL (green), mPFC (magenta), and MC (orange) during classical eyeblink conditioning. (*A*) Mean power spectra of LFPs recorded in the three recording sites between 1.5 s before and 2 s after the CS initiation during the second habituation session (HAB02). Black arrows indicate spectral ranges corresponding to delta (1–5 Hz), theta (5–12 Hz), beta (12–35 Hz), and low- (35–50 Hz) and high- (50–100) gamma bands. (*B*) Histograms of mean spectral powers for all frequency bands. Baseline values (collected from HAB02 sessions, including no stimulus) are also represented (dotted black line inside the bars); note that they are very similar to those collected during the presentation of the unpaired CS (HAB02). (*C*) Spectrograms corresponding to data illustrated in *A*, *B*. Note that the maximum values of spectral power (see the color calibration bar at the right) appeared during and after CS presentations, and the fundamental contribution to the spectral power was determined by delta and theta bands. (*D–L*) Same representations and analyses for LFPs recorded in CL, mPFC, and MC during phase I (*D–F*), phase II (*G–I*), and phase III (*J–L*). Note that the most-prominent and -differentiated power peaks appeared in delta, theta (white arrows in the spectrograms), and low gamma (black arrows in the spectrograms) bands for the mPFC and CL spectra during conditioning phases I and III (but not during phase II, just when CL neuron activation reached its maximum firing rates). This suggests the possibility of delta–gamma comodulations in *D* and *J* but uncorrelated rhythms in panel *G*. For all the multiple comparisons (Tukey–Kramer test: *$P < 0.05$; **$P < 0.01$; ***$P < 0.001$).
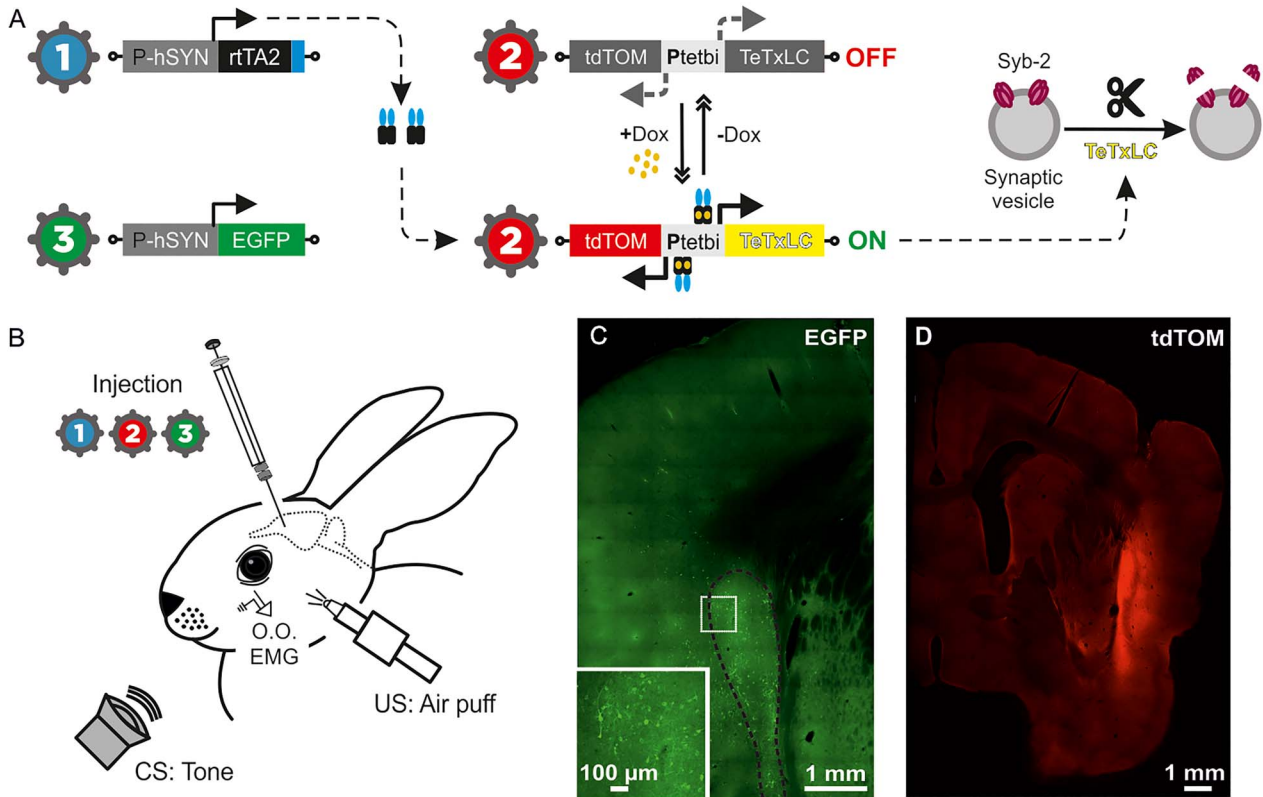
Figure 7. Animal preparation for classical eyeblink conditioning following virus-delivered inducible silencing of synaptic transmission (vINSIST) of CL neurons. (A) The three injected viruses were as follows: (1) rAAV–P_{hSYN}–rtTA; (2) rAAV–P_{tet}bi–TeTxLC/tdTOM; and (3) rAAV–P_{hSYN}–EGFP. With the vINSIST method, the reverse tetracycline trans activator (rtTA) is expressed under a human synapsin specific promoter (P_{hSYN}) and the tetanus toxin light chain (TeTxLC) and tdTomato (tdTOM) are under a bidirectional tet responder promoter (P_{tet}bi). Only under doxycycline (Dox) treatment, rtTA binds the P_{tet}bi to express simultaneously TeTxLC, which blocks synaptic transmission, and tdTOM, a tracer that we used to identify the inhibited zone. Virus 3 acted as a post hoc histological tracer for validating the degree of precision and the expression of rtTA. (B) Diagram illustrating the animal's injections with the rAAVs and its preparation for the classical conditioning of eyelid responses. (C) Photomicrographs from CL infected neurons glowing green due to EGFP fluorescent protein generated by the administered virus 3. The large white square is an amplification of the smaller one. (D) Photomicrograph from the inhibited CL glowing red due to tdTOM fluorescent protein generated by the activation of the P_{tet}bi by dox administration.

Results

Location and Identification of Claustral Neurons

Because of its substantial connectivity with the MC, the CC, and the mPFC (Kowiański et al. 1997; Majak et al. 2000; Smith and Alloway 2010; Mathur 2014; White et al. 2018; Smith et al. 2019) and its significantly larger size, the rostral and central portion of the dorsal CL was targeted for electrophysiological recordings. In accordance with Kowiański et al. 1997, that region in rabbits corresponds mainly to the somatosensory and motor protection zones, perhaps also including the auditory and PFC projections areas. The recording area was initially approached using available stereotaxic coordinates (Girgis and Shih-Chang 1981). As illustrated in Figure 1E, recorded neurons were identified by their orthodromic (i.e., synaptic) activation from the MC and the mPFC. Occasionally, they were also activated from the CC (not illustrated). In the absence of conditioning stimuli, the spontaneous activity of CL neurons recorded here ($n = 315$ from seven rabbits) presented irregular, low firing rates (5–25 spikes/s). Synaptic and/or antidromic activation was recorded when stimulating MC, mPFC, or CC in 81.90% (258/315) of the cases (Supplementary Table 1).

The electrical stimulation of either MC evoked a characteristic early (~10 ms) and late (~150 ms) activation of most (contralateral: 39.44%; ipsilateral: 66.9%) CL neurons, including a noticeable intermediate silent period (Fig. 1E1,G2). Repeated MC stimulations (at 0.1 Hz) increased the mean firing rate of CL neurons (to 50 spikes/s) for the ~300 ms following the silent period. CL neurons (15.59%) were also antidromically activated from the ipsilateral MC with the help of the collision test (Fig. 1G1, see Methods). Mean activation latencies were 3.12 ± 0.13 ms (mean $\pm$ SEM; $n = 20$; range: 2.02–4.53 ms). Additional support for the antidromic nature of spike activation was that it followed stimulation frequencies of up to 300 Hz. Finally, the electrical stimulation of either of the two implanted mPFC sites drove preferentially neurons located deeper in the CL (contralateral: 9.15%; ipsilateral: 10.06%) with a similar profile (i.e., short, late activations separated by a silent period; Fig. 1E2), but with a longer activation latency and a smaller increase in the firing rates of the activated neurons (to 25 spikes/s). With regard to the CL neurons stimulated ipsilaterally from CC, almost half of them (44%) responded to stimuli presented to the rostral CC (AP: 4 mm) and 32% to the caudal part (AP: 0 mm). They were also activated antidromically in 9.09% of the cases from the

rostral CC and in 12.5% of the cases from its caudal part, suggesting the presence of bidirectional projections between CL and CC (Chia et al. 2020).

Small electrolytic-lesion marks made with tungsten electrodes at the end of the recording sessions indicated that recorded neurons occupied a dorsal position in the rostral part of the CL (Fig. 1C,D). With the help of these electrolytic marks and collected information regarding stereotaxic coordinates, we show the location of recorded CL neurons ($n = 315$) included in this study. Figure 1D illustrates that the recorded neurons formed a cell column (AP: 0–3 mm; L: 5.5–6.25 mm) in between the striatum and the insular cortex. Note that in its thickest portion, the size of rabbit CL can be ~1 mm (Kowiański et al. 1999).

As previously reported (Ammann et al. 2016), the MC area that we stimulated was clearly related to eyelid movements: stimulation there (twin pulses separated by a 2 ms interval) evoked short-latency activation (16.6 ± 0.4 ms; range 15.1–18.7 ms) of the contralateral O.O. muscle (Fig. 1F3). In contrast, applying similar stimuli to the CL (Fig. 1F1), mPFC (Fig. 1F2), or CC (not illustrated) did not activate this muscle.

Firing Activity of Claustral Neurons During Classical Eyeblink Conditioning

For eyeblink conditioning, animals were presented with a tone as CS and, 250 ms later, with a 100 ms air puff aimed at the left cornea as US (Fig. 2A,B). Apart from two preliminary recording sessions to adapt the animals to the recording devices, activity of CL neurons was recorded for two habituation sessions (only CS was presented) and eight conditioning sessions (paired CS/US, $n = 5$), or six pseudoconditioning sessions (randomized CS and US, $n = 2$). Mean learning curves of conditioned and pseudoconditioned animals are illustrated in Figure 2C. Although conditioned animals reached the selected criterion by the fifth session, training was maintained up to the eighth session. The aim was to identify and record neurons both during the acquisition process and when the learning curve reached asymptotic values. Those acquisition values were similar to those collected in rabbits when using the same delay conditioning paradigm and recording characteristics (Gruart et al. 2000; Leal-Campanario et al. 2007; Caro-Martín et al. 2015; Ammann et al. 2016).

Neurons were classified in three different groups (A–C) depending on their firing activity during presentations of paired stimuli (Figs 2B, 3A–C and Supplementary Table 2). The following analysis only includes neurons recorded for ≥8 trials during conditioning ($n = 130$ neurons from $n = 5$ rabbits) or pseudoconditioning sessions ($n = 47$ neurons from $n = 2$ rabbits); otherwise, sorting them depending on their activity was very ambiguous. All the selected neurons were also activated by at least one of the stimulating electrodes (MC, mPFC, and/or CC) to ensure that the recording site was the CL.

Type A neurons recorded during conditioning sessions ($n = 59$) were characterized by a >30% increase in their firing rate during CS/US presentations and even after them (Figs 2B and 3A). In the absence of the paired stimuli, type A neurons presented an irregular, low (15–20 spikes/s) discharge rate. Type A neurons were rarely activated during single-stimulus presentations of any sensory modality. As a whole, the averaged firing rate of type A neurons increased $293.02 \pm 29.56\%$ compared with baseline values acquired immediately before CS presentations ($H = 50.900$ with one degree of freedom; $P < 0.001$; Kruskal–Wallis one-way ANOVA on ranks). The activation of these neurons took place

175.5 ± 11.5 ms ($n = 57$; range 50–430 ms) after the CS presentation—namely, well after the mean value for the beginning of CRs (156.7 ± 13.8; range 76–231 ms). The activation lasted 476.8 ± 33.5 ms, that is, very much longer than the CS + US interval. In addition, the mean peak activity of type A neurons took place slightly after the CS/US presentations (380 ± 39.5 ms after CS onset). In Figure 2B is illustrated a type A neuron recorded from a well-trained animal during the fifth conditioning session. The cell was activated after CR initiation (i.e., 164 and 129 ms after CS onset, respectively). The averaged firing rate of this neuron increased 330.43% steadily from its early activation until surpassing the end of the US by >600 ms [$F_{(1,8)} = 58.533$; $P < 0.001$; one-way ANOVA F-test]. Its firing rate peaked right before (229 ms after the CS) the US presentation and reached ~50 spikes/s. In contrast, the type A neuron illustrated in Figure 3A started increasing its firing rate almost at the same time as CR onset (~160 ms after the CS) but also reached its peak firing rate before the US (208 ms). Here again, the increase in firing rate (593.51% more than its baseline) surpassed the end of the US by >600 ms [$F_{(1,8)} = 80.365$; $P < 0.001$; one-way ANOVA F-test].

Type B neurons recorded during conditioning sessions ($n = 16$) were characterized by a ≥30% decrease in their firing rate during CS/US presentations (Fig. 3B). In the absence of paired stimuli, type B neurons presented an irregular spontaneous firing rate (20–30 spikes/s), some 133–150% higher than that presented by type A neurons. As already described for type A neurons, type B cells were rarely found during single-stimulus presentations of any sensory modality. The averaged firing rate of type B neurons decreased $59.59 \pm 5.82\%$ compared with baseline values ($H = 38.434$ with one degree of freedom; $P < 0.001$; Kruskal–Wallis one-way ANOVA on ranks). Overall, the inhibition of type B neurons took place from 60.0 ± 18.7 to 266.6 ± 25.2 ms after CS presentations (mostly during the CS–US interval); hence, their inhibition occurred before the mean value for the beginning of CRs (156.7 ± 13.8; range 76–231 ms). As an example, Figure 3B illustrates a type B neuron recorded from a well-trained animal during the eighth conditioning session. This neuron was inhibited 65 ms following CS presentation, well before CR onset (111 ms after the CS) and recovered its baseline activity (~250 ms after the CS); that is, by US presentation. This neuron presented a decrease of 79.16% of its activity during approximately 185 ms [$F_{(1,7)} = 62.395$; $P < 0.001$; one-way ANOVA F-test].

Type C neurons recorded during conditioning sessions ($n = 55$) presented an irregular firing rate (20–30 spikes/s) that was not modified by any stimulus present in the recording room, including the paired CS/US presentation during conditioning sessions ($H = 0.678$ with one degree of freedom; $P = 0.41$; Kruskal–Wallis one-way ANOVA on ranks). See an example in Figure 3C. This neuron did not change its firing rate in response to CS/US presentations; its baseline values—obtained 500 ms before CS onset—were very similar to those obtained 500 ms after the CS (25.74 and 26.50 spikes/s respectively) [$F_{(1,8)} = 0.127$; $P = 0.731$; one-way ANOVA F-test].

Remarkably, the percentage of these three types of neuron was modified across habituation and conditioning sessions but not during pseudoconditioning. As illustrated in Figure 3D, the evolution in the relative percentage of type A (green), B (red), and C (blue) neurons across training was best represented with quadratic or higher order polynomial fits (Supplementary Table 3). Thus, during the two habituation sessions, type C neurons represented 68.42% and 83.33% of recorded units, respectively, while type A neurons were only 26.32% and 16.67%, and type B less than 5%. During the first

five conditioning sessions (prelearning and learning phase, up until rabbits reached the selected criterion), these percentages changed notably for types A and C neurons. The number of type A neurons showed a growing trend, reaching its highest value around CON05 and reaching values of 76.47% of recorded units. In contrast, the number of type C neurons decreased, showing its lowest value also at CON05 (11.76%). From CON06 on (when the percentage of CRs reached asymptotic values), this trend flipped again, and by CON08 type C neurons were the most numerous cells recorded (46.15% for type C; 38.46% for type A). Type B cells presented rather low, constant values (12.27 ± 2.26%, ranging from 0 to 25% of recorded units) across sessions, and no trend was detected.

As indicated in Figure 3E,F and Supplementary Table 3, no changes in the relative percentages of types A, B, and C neurons were observed during pseudoconditioning sessions. In response to single CS presentations, the percentage of the recorded type C neurons remained at high levels, while the percentages of types A and B neurons maintained low levels across training [Fig. 3E, types A (10.64%), B (4.26%), and C (85.11%)]. Similar results were collected during single US presentations [Fig. 3F, types A (12.5%), B (2.5%), and C (85%)]. The reliability of these data is confirmed by the results obtained for the two habituation sessions when only the CS was presented (Fig. 3D,E).

Taken together, recorded CL cells did not respond to single stimuli (even when presented at high intensities), as during pseudoconditioning. Type A neurons did respond with an increase of firing activity to the same stimuli when they were presented together (paired CS/US); in this situation, their percentage increased in conjunction with the development of CRs, until animals reached the learning criterion—that is, when the acquisition phase was finished. The burst of activity presented by type A neurons followed the initiation of CRs. In contrast, type B neurons decreased their activity during the CS–US interval, but the number of recorded units remained low across sessions and no particular evolution was observed. Their inhibition preceded CR onset. Interestingly, the number of recorded neurons not related to CS and US presentations (type C) decreased during the first conditioning sessions until animals reached criterion. This suggests a recruitment of type A CL neurons, at the expense of type C cells, during CR acquisition.

Because firing rate profiles and spike durations vary between pyramidal cells and interneurons (Buzsáki and Kandel 1998; Csicsvari et al. 1999; Constantinidis and Goldman-Rakic 2002; Barthó et al. 2004; Viskontas et al. 2007), we used these two criteria to discriminate principal (projecting neurons) and nonprincipal units (putative inhibitory interneurons) from neuronal recordings. Following the analytical procedures detailed in Supplementary Table 4, Supplementary Fig. 3, and Supplementary Appendix 2, no significant differences ($P > 0.05$) were observed between the spike durations of types A and C neurons. Only the cluster of spikes from type B neurons showed shorter spike durations (0.88 ± 0.01, range 0.80–0.92 ms) than those of type A cluster (1.04 ± 0.01, range 0.94–1.09 ms). The multiple comparison demonstrated that there was a statistically significant difference ($H = 16.26$ with one degree of freedom; $P < 0.001$; Kruskal–Wallis one-way ANOVA on ranks) between the mean values of the spike duration (see Supplementary Table 4). These differences in spike duration together with their different firing patterns, suggest that type B neurons could represent a population of CL interneurons, while types A and C neurons might represent projecting neurons.

Changes in the Firing Rate of Type A Neurons in Relation to the Development of Conditioned Responses Across Conditioning

We also checked the putative relationships between the discharge rates of type A neurons during the acquisition process and EMG activity of the left O.O. muscle collected during the corresponding sessions and trials (Fig. 4). For this, we quantified the integrated firing rate [in (spikes/s) × s] of type A neurons during the CS–US (Fig. 4A,B,D) and CS + US (Fig. 4A,C,E) periods and represented it against the EMG area (in mV × s) of the rectified EMG activity of the left O.O. muscle ($n = 5$ animals; Supplementary Table 5). We determined the linear relationships between these two variables in early (from first to third) and late (from fourth to eighth) conditioning sessions during the CS–US interval (early conditioning, Fig. 4B; late conditioning, Fig. 4D), and also during the CS + US period (early conditioning, Fig. 4C; late conditioning, Fig. 4E). None of these four representations (Fig. 4B–E) indicated the presence of a linear relationship ($r \geq 0.6$).

Finally, it is well known that training reduces the latency of CRs with respect to CS presentation (see details and references in Gruart et al. 1995). If claustral neuron activity is related to the development and/or expression of CRs then type A neurons in well-trained animals should decrease their initiation latency with respect to CS onset. Accordingly, we checked whether the activation latency of type A neurons to CS presentation was inversely correlated to the percentage of CRs. As illustrated in Figure 4F, we found that there was no linear relationship between these two variables. Taken together, these results indicate that type A neurons are not related with the EMG activity of the O.O. muscle during the acquisition process.

Analysis of LFPs Recorded in CL, MC, and mPFC During the Classical Conditioning of Eyelid Responses

During the unitary recording sessions, we noticed the presence of specific changes in LFPs recorded in the CL across conditioning, particularly in the gamma band (Cebolla and Cheron 2019). In order to have consistent recordings of selected CL sites during all training sessions, we prepared four additional rabbits with chronically implanted tetrodes in the right CL (Supplementary Fig. 1D). For comparative purposes, those animals were also chronically implanted with recording bipolar electrodes in mPFC and MC (Supplementary Fig. 1D). To avoid any distortion of LFP recordings, no electrical stimulation of the implanted sites was carried out in this group of animals.

Representative LFPs collected from CL, MC, and mPFC are shown in Supplementary Figure 1A,B. Those examples exhibit 3.5 s frames (from 1.5 s before to 2 s after CS presentations) taken from the second habituation (Supplementary Fig. 1A) and the eighth conditioning sessions (Supplementary Fig. 1B). It can be seen that conditioning increases LFP amplitudes in the three recording sites and evokes the presence of a high-frequency oscillation following the paired CS/US presentation in CL and mPFC recorded traces (Supplementary Fig. 1B).

Figures 5 and 6 illustrate the spectral analysis of LFPs (in 3.5 s frames, as those shown in Supplementary Fig. 1A,B) recorded during baseline and the second habituation session, and also during three conditioning sessions that represent different learning stages (Supplementary Fig. 1C): phase I (before learning, <12% of CRs, 5.95 ± 2.16%; mean ± SEM); phase II (during acquisition, ~50% of CRs, 47.45 ± 2.93%); and phase III (after learning, >85% of CRs, 94.27 ± 2.22%). Those phases

were selected following a previous study from our laboratory (Fernández-Lamo et al. 2018). Time frames from phases I to III included the paired CS/US presentations, while habituation sessions included only the CS, and baseline sessions did not include any stimulus.

Figure 5 shows the results for the analysis of the LFP recordings carried out in the CL. As plotted in Figure 5A,B, baseline and habituation did not show any difference in the mean spectral power of the five selected bands [delta (1–5 Hz), theta (5–12 Hz), beta (12–35 Hz), low gamma (35–50 Hz), and high gamma (50–100 Hz)], whereas during the conditioning phases it increased significantly in all the frequency bands (Tukey–Kramer multiple comparison test: HAB02 and Baseline vs. phases I, II, and III; $P < 0.001$; ***).

Following Fernández-Lamo et al. (2016), for a more-precise dynamic analysis of spectral powers computed from LFPs, we selected moving time-windows of 500 ms (shifted in 10 ms increments) and we calculated multitapered Fourier transforms. Thus, time–frequency representations were computed for the 3.5 s LFP frames recorded in the CL for habituation and phases I, II, and III (Fig. 5C). The illustrated spectrograms correspond to 600 tapered Fourier transforms, each corresponding to the average of 120 frames × 5 tapers. Collected results indicate that the maximum power values appeared during the CS + US interval and 0.75 s following it, throughout the subsequent conditioning phases. This is particularly visible in lower frequency bands (delta, theta; Fig. 5C, white arrows), but it is also present in the higher frequency bands (beta, low gamma and high gamma). Likewise, notice the increase of the spectral power in the low gamma band 1 s after the CS/US presentation shown in phases I and III spectrograms, but not in phase II (Fig. 5C, black arrows).

Figure 5D represents probabilistic maps for the multiple comparisons between pairs of spectrograms, where red (inference type +1) and blue (inference type −1) indicate significant statistical differences ($P < 0.05$; jackknifed estimates of the variance), and white (inference type 0) indicates no significant differences ($P > 0.05$). It can be seen clearly that spectral powers of LFPs recorded during conditioning sessions were higher than those recorded during habituation (red, inference type +1), mainly during and after CS/US presentations. Specific differences were observed when comparing the three selected conditioning phases: between phases I and III versus phase II, mainly in low gamma band (see the black arrows 1 s after the CS/US presentation), and between phases I and II versus phase III for low frequencies (red arrows). The probability density histograms (Fig. 5E) allowed us to verify the aforementioned results.

It is noticeable in all the representations (Fig. 5A–D) that spectral power of phase II is the highest in low frequencies before and during the CS/US presentations (in which is similar to phase I). In contrast, the peak in low gamma frequency 1 s after the CS/US present in phases I and III is missing in phase II. The increment of the low gamma spectral power during phases I and III respect to phase II in this specific temporal range (between 1 and 2 s after CS presentation) could be a CL cognitive-control inference.

Alternatively, Figure 6 illustrates a comparative spectral analysis of the LFPs recordings carried out in CL (green), mPFC (magenta), and MC (orange) simultaneously. Figure 6A–C shows mean spectra (A), histograms of mean spectral power (B), and time–frequency spectrograms (C) of these tree recording sites during habituation. Figure 6, D–FG–I and J–L provides the same information about conditioning phases I, II, and III respectively. In addition, in the multiple comparison histograms

(Fig. 6B,E,H,K), the difference to the baseline values is shown (dotted black line). The histograms also further illustrate that the above-indicated changes in spectral power for LFPs collected in the CL when comparing habituation versus any of the conditioning phases were present in mPFC and MC as well, and they were even stronger (Tukey–Kramer multiple comparison test: HAB02 and Baseline vs. phases I, II, and III; $P < 0.001$, white asterisk).

CL results were detailly described and analyzed above, hence data from mPFC and MC LFP recordings are going to be evaluated next. The changes we observed in CL LPF spectra seem to be present and even greater in mPFC ones. Apparently, both structures follow a similar spectral pattern. The two structures increased their LFP spectral power in delta (1–5 Hz) during phases I and II (even though both increased, power values from mPFC became statistically different that those from CL, $P < 0.001$), and reduced it notably in phase III. In addition, they both raised remarkably their spectral power for low gamma band (35–50 Hz) in phases I and III (Fig. 6E,K, 35–50 Hz plots; Fig. 6F,L, see black arrows). Curiously, mPFC is the one recording site whose theta band (5–12 Hz) spectral powers grew the most compared with habituation session, but its values remained unchangeable throughout the three conditioning phases. On the other hand, LFP recordings from MC did not follow the same spectral patterns as those from CL and mPFC. Its spectral powers did increase in phases I and II specially for low frequencies (delta and theta), but in contrapositions to CL and mPFC, LFP from MC did not experience any noticeable change for the low gamma values across phases I, II, and III (*$P < 0.05$; **$P < 0.01$; ***$P < 0.001$; Tukey–Kramer test).

None of the three structures presented any remarkable change in beta (12–35 Hz) and high gamma (50–100 Hz) bands, except the general increase of spectral power in all the five bands produced presumably due to the conditioning itself.

Finally, comodulation analysis by means of the crossfrequency couplings and the computation of the power–power spectral ratios between different frequency bands indicated that the strength of these crossfrequency interactions changes dynamically and differentially, between the LFP oscillatory activities from CL, mPFC, or MC. In summary, the LFP oscillatory patterns at CL–mPFC network nodes were correlated with coordinated dynamic changes in delta and low-gamma powers. In contrast, at the CL–MC network nodes, the power dynamics in delta and gamma frequency bands were uncorrelated. In relation to the above, see further comments and detailed statistical results in Supplementary Appendix 3.

Effects of Blocking CL Output on the Acquisition Curve and on the EMG Activity of the Orbicularis Oculi Muscle During Classical Eyeblink Conditioning

In a final experimental step, we studied the putative effects of blocking CL neuron output on learning and/or performance of conditioned eyeblink responses. For this, we used a novel method for virus-delivered inducible silencing of synaptic transmission (vINSIST, see Methods, and Supplementary Fig. 2 and Supplementary Appendix 1). A homogeneous cocktail of three rAAVs was injected at three different sites (2 μL each) in the two CLs (Fig. 7). With the vINSIST method, we were able not only to silence the synaptic transmission in CL after doxycycline treatment, but also to target infected (EGFP, green) and inhibited (tdTOM, red) CL neurons (Fig. 7C).
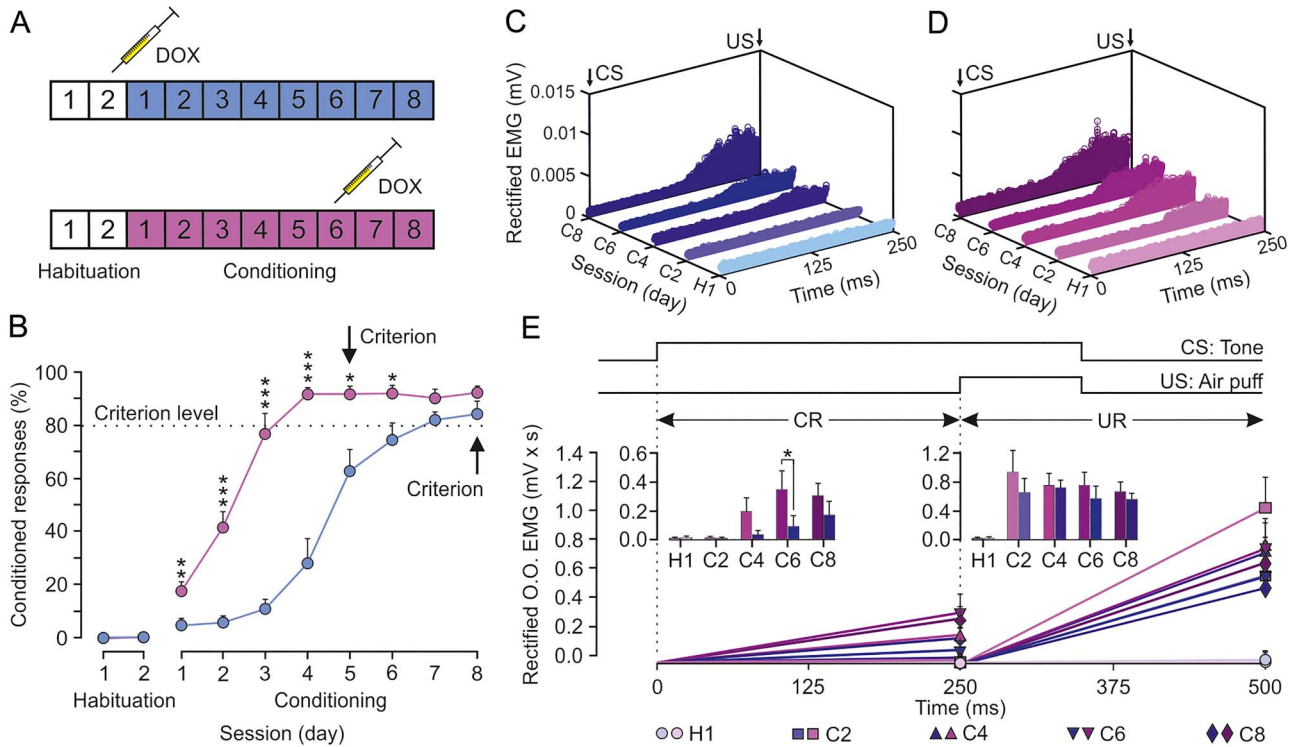
Figure 8. Classical conditioning of eyelid responses during the inhibition of both CLs. CL neurons were inhibited by the local injection of a cocktail of rAAVs equipped with doxycycline (Dox)-dependent tetracycline-controlled genetic switches, which release tetanus toxin (TeTxLC) when activated. (A) Animals ($n = 8$) were classically conditioned using a delay paradigm following two protocols: half of them (blue group) were injected with Dox after the second habituation session and the other half (magenta group) after the sixth conditioning session. (B) Learning curves corresponding to the two groups of animals. Data are presented as mean ± SEM (see the multiple comparison reports: *$P < 0.05$; **$P < 0.01$; ***$P < 0.001$; Holm–Sidak or Tukey–Kramer tests). (C) Rectified EMG activity of the left O.O. muscle from the blue group during the CS–US interval (CRs time gap) and collected for the indicated habituation and conditioning sessions ($n = 50$ trials per session from $n = 4$ animals). (D) Same representation for magenta group. Note the earlier and larger CRs attained by this group during CS–US interval. (E) Quantitative analysis of cumulative areas (in mV × ms) of the rectified EMG activity of the left O.O. muscle recorded during the CS–US interval (CR time gap) and during the 250 ms following it (CS + US interval plus 150 ms, UR time gap) for the five indicated sessions. The insets illustrate the differences in net EMG areas between the two groups (*$P < 0.05$) during the CS–US (CRs) and the CS + US intervals (URs). No differences were found between groups for URs.

A total of eight rAAV-injected rabbits were classically conditioned using a delay paradigm; four of them were injected with doxycycline following the second habituation session (before the learning has even started; the blue group) and the other four were injected following the sixth conditioning session (after the learning has been achieved; the magenta group) (Fig. 8A). As illustrated in Figure 8B, animals included in the early inhibited CLs group (blue) presented a significantly delayed learning curve [$F_{(7,42)} = 14.179$; $P < 0.001$; two-way ANOVA F-test, with one factor repetition] with respect to values collected from the late-inhibited CLs group (magenta). In contrast, the activation of the injected rAAVs in the magenta group after the sixth conditioning session (i.e., once the learning criterion has been reached) produced no noticeable effects.

In regard to the EMG activity of the O.O. muscle during the CS–US interval (Fig. 8C–E), the early inactivation of both CLs in the blue group significantly decreased the mean area of the rectified EMG during the intermediate conditioning sessions, but control values were reached by the eighth conditioning session [$F_{(3,18)} = 7.287$; $P = 0.002$; two-way ANOVA F-test, with one factor repetition; see inset in Fig. 8E]. In contrast, there were no significant differences for the evoked URs shown during the CS + US period [$F_{(3,18)} = 3.036$; $P = 0.056$; two-way ANOVA F-test, with one factor repetition].

In summary, the early inactivation of both CLs delayed the acquisition of a classical conditioning task without affecting its performance, but their inactivation in well-trained animals had no effect. Therefore, we conclude that CL neurons are involved in the cognitive component of the eyeblink conditioning, rather that the motor.

Discussion

We have found that CL neurons exhibit changes in their activity during classical eyeblink conditioning in behaving rabbits. Their firing properties were related to cognitive aspects of the acquisition process rather than the kinematics of the CR. Below we discuss our findings in detail and consider the potential role of the CL in cognitive-like functions involved in associative learning.

Location and Identification of Claustral Neurons

Specific details were considered to ensure that recordings were carried out in the CL. Even though rabbit CL is far easier to access, due to its significantly larger size (compared with mouse CL), its differential and dense connectivity (anti- and ortho-dromic) with MC, mPFC, and CC (Carman et al. 1964; Crick and Koch 2005;

Mathur 2014; Chia et al. 2017; Atlan et al. 2018; White et al. 2018) and its spontaneous firing rate (Spector et al. 1974; Chachich and Powell 2004) are key to identifying the recorded zone. The electrolytic marks in the postmortem tissues confirmed that the region recorded was the CL.

CL neurons were easily activated synaptically from MC, mPFC, and CC, but their antidromic activation was much more difficult. This could be the result of their extensive branching into different cortical areas (Marchi et al. 1983; Minciacchi et al. 1985; Majak et al. 2000), which would certainly hinder the antidromic invasion of their somas (Steriade et al. 1971; Lipski 1981). As supported by the present results and in the multiunit recordings carried out in rabbit CL during Pavlovian heart rate conditioning by Chachich and Powell (2004), CL neurons presented a low, irregular spontaneous firing that was not easily modulated by the single presentation of stimuli used as CS or US. This characteristic firing helped to differentiate CL from nearby nuclei while recording. For instance, insular neurons in rabbits present inconstant, low-magnitude responses during classical conditioning (Gibbs et al. 1992). Moreover, insular neurons in monkeys seem to be involved in integrative complex processing of sounds and vocal communications (Remedios et al. 2009), while—as reported here—CL neurons are not very active when presented with single stimuli of any sensory modality. Finally, the inactivation of the insular cortex by tetrodotoxin evokes different effects to those reported here for the CL (Bermudez-Rattoni et al. 1991). On the other hand, striatal cells present a characteristic low-frequency stable tonic firing that can be modulated during classical eyeblink conditioning but with response profiles pretty different (Blázquez et al. 2002) to those reported here for types A and B neurons.

Finally, action potentials recorded in fiber tracks and long dendrites present a quite different shape than those recorded near neuron somas (Delgado-García et al. 1990; Deligkaris et al. 2016). That is why we dismiss the possibility of having been recording in the extreme or external capsule or dendrites located outside the nucleus. Thus, we are positive that the neuronal activity analyzed in this work has been recorded in the CL.

Firing Activity of Claustral Neurons During Classical Eyeblink Conditioning

Type A neurons reported here presented activation profiles similarly to those of other cortical neurons recorded in rabbits during delay eyeblink conditioning. For instance, Leal-Campanario et al. (2013) identified mPFC pyramidal neurons that presented a delayed firing with respect to CS presentation. Caro-Martín et al. 2015 ("late mPFC neurons") and Ammann et al. 2016 ("type C pyramidal MC neurons") also recorded similar cells. In addition, CL neurons recorded by Chachich and Powell (2004) presented a late and longer lasting increase in their discharge rate during paired CS/US presentations similarly to type A neurons reported here. In contrast, they did not report the presence of cells that responded with inhibition (type B neurons), probably due to their multiunit recording procedures. Even using single-unit recordings as carried out here, finding type B neurons was challenging. Inhibition was perceptible only when neurons had high baseline firing rates and the recording was held for a long time. Type C neurons did not respond to any stimuli, not even to the paired CS/US presentations. They represented more than 75% of the recorded cells during habituation and pseudoconditioning sessions (when single or unpaired stimuli were presented), but they became less frequent during the learning phase. In fact,

they seemed to be replaced by type A neurons, whose number increased considerably (Fig. 3D–F). Although the spike durations of types A and C neurons were similar and they presented an inverse relation across conditioning, the fact that they presented different baseline firing rates prevent considering them as member of the same CL population.

Moreover, this work clearly shows how types A and B neurons respond to the presentations of the paired CS/US. Therefore, we believe they must play a role in this type of associative learning. Claustral type A neurons increased their activity with the association of the paired CS/US during the acquisition of the CRs. However, we reject the possibility that their function during the learning phase is related to the motor performance of the CRs, for three main reasons: (1) CRs appeared mostly before type A neurons discharged (156.7 ± 13.8 and 175.5 ± 11.5 ms after the CS, respectively), so there is no way their activation could produce or modulate the movement of the eyelid. (2) The first CRs started appearing very soon in the training and they became larger and more numerous until the learning curve reached asymptotic values (around the fifth session). If type A neurons were necessary for the proper execution of the CRs, their activation should be maintained specifically during the last conditioning sessions, when more and bigger CRs are delivered. On the contrary, these data show that after the fifth session, type A neuron number starts to decrease (Fig. 3D). And (3) the regression analysis dismisses any linear relationship between the discharge rates of type A neurons and the EMG activity of the O.O. muscle ($r \geq 0.6$), both for the CS–US period, where CRs are expected (Fig. 4B,D,F) and for the CS + US interval, when URs appeared (Fig. 4C,E). On top of that, it was usual to find CS/US trials with type A neuron firing activity and no CR, and vice versa. It can be concluded then that type A neurons are not related to the correct performance of the eyelid CRs. Alternatively, it is more plausible that their role is related to attentional, cognitive processes, since type A cell activity is mainly required during the acquisition phase: once the CRs are fully developed and the learning is achieved, no more activation in the CL is recorded. Furthermore, claustrocortical connections are expected to produce inhibition of their target cortices, especially in PFC (Jackson et al. 2018). Therefore, we hypothesize that type A cell activity will suppress cortical areas during the learning phase.

In contrast, given their firing profiles during conditioning and the short duration of their spikes, type B neurons are expected to be interneurons and not project out of the CL. They certainly did respond to the CS/US before the initiation of the CRs (60 ± 18 and 156.7 ± 13.8 ms after the CS, respectively), but it is unlikely that their inhibition is somehow involved in the CR performances. Rather, they might be part of an inhibitory inner circuitry. Anyhow, as said before, more data are needed to clarify with regard to type B neurons.

Analysis of LFPs Recorded in CL, MC, and mPFC During the Classical Conditioning of Eyelid Responses

According to data obtained from LFPs recorded in CL (Fig. 5), habituation and baseline results barely differed, and single CS presentations did not produce any change in spectral power, as has already been indicated for single-unit recordings. In contrast, the CS/US association increased the spectral power of all the frequency bands. Comparing spectral power changes (Fig. 5C) with single-unit activation (Fig. 3D) throughout phases I, II, and III, we noticed several remarkable details: (1) In the prelearning stage (phase I), there was a perceptible increase of

low-frequency (delta and theta) spectral powers, and simultaneously (during and slightly after the CS/US presentation) a few type A neurons started firing. One second after the CS, there was a slight increase of low gamma spectral power. (2) During the acquisition stage (phase II), delta and theta spectral powers were the highest simultaneously (during and slightly after the CS/US presentation) with the increased firing of type A neurons. One second after the CS, the low gamma peak had disappeared. And (3) when learning had been achieved (phase III), delta and theta presented the lowest spectral powers during and slightly after the CS/US, while type A neurons were rarely recorded. Yet, one second after the CS, the low gamma band presented its highest value, with a prominent peak.

To sum up, the spectral patterns (power–power ratios and amplitude–amplitude comodulations) suggest that the couplings in which delta–gamma comodulation appears in CL LFPs seem to depend on the learning phase. Not only are they absent during habituation sessions, but also, the strength of these crossfrequency interactions changed differentially during phases I, II, and III. Moreover, those patterns seem to be tightly related to the single-unit activities. Available information concerning LFP recordings carried out in CL of behaving rats indicates a similar modulation between two frequency bands (1–4 and 8–12 Hz) during spontaneous behaviors (Jankowski et al. 2017), although frequency bands in rats and rabbits are not equivalent.

Data collected from LFP recordings carried out in CL, mPFC, and MC are quite intriguing. Despite the fact that MC recordings seem to follow a completely different pattern, mPFC recordings also presented a distinctive increment of spectral power in low-gamma frequencies during some conditioning phases, as described above for CL recordings. Thus, LFPs recorded from CL–mPFC network nodes show an amplitude–amplitude coupling between delta and low-gamma frequency bands during phases I and III. In contrast, during the acquisition stage (phase II) the low gamma peak disappeared in CL and mPFC and delta–gamma comodulation was not found. In single-unit recording experiments, it was also during the acquisition sessions that the percentage of type A neurons was greater, reaching its highest value at the end of this stage (Fig. 3D). These cells fired from 175.5 ± 11.5 to 476.8 ± 33.5 ms after the CS presentations and ≈500 ms after that, the expected low-gamma peak was missing. Thus, firing activities of CL neurons could prevent the presence of low-gamma oscillations. Additionally, as Jackson et al. (2018) have reported using optogenetic activation of CL neurons, it is likely that CL type A cells target mPFC interneurons which inhibit pyramidal neurons. Those inhibited mPFC neurons could generate the low-gamma oscillations described in phases I and III (especially considering that spectral power values for low gamma were higher in mPFC than in CL). After the acquisition period (i.e., in phase III), CL neurons become silent and mPFC might again generate low gamma oscillations. This would also explain why in phase I, the low-gamma peak is small: there are already a few CL neurons firing, but not sufficient to inhibit PFC activity as they do in phase II.

In contrast, MC does increase its spectral power values for low frequencies (delta and theta) across conditioning, but not for low gamma. This fact helps to verify that this peak in the low-gamma band is specific and is not occurring all-brain-wide due to signal contamination. In accordance, it can be suggested that the power dynamics at CL nodes could be related to cognitive-like functions (CL and mPFC LFPs are correlated) rather than to the motor neural control (CL and MC LFPs are uncorrelated)

during classical eyeblink conditioning (contrary to the predominant motor control role played by MC circuits for the generation of eyelid-conditioned responses (CRs) as described by Ammann et al. 2016).

Notice that for LFP experiments, we use special electrodes to avoid multiunitary recording that could affect low- and/or high-gamma amplitudes. Thus, the delta–gamma couplings in the CL–mPFC network nodes were due to genuine interactions between spectral patterns of two LFP oscillations, and not to spike contamination from the local firing of CL and/or mPFC neurons. These LFP spectral patterns should endorse the proposal of the delta-associated gamma oscillations described here as a new type of CL–mPFC coupling, directly involved in cognitive processes related to this type of associative learning. Indeed, results presented here further support evidence (White et al. 2018) of a cognitive control system, where CL is subservient to network function (mainly top–down) rather than an integrator of sensory cortical information.

CL Inactivation Delayed Learning During Classical Eyeblink Conditioning

Regarding the inhibition of CL neuron afferences, the injections of the vINSIST rAAVs were minimal and local, in order to avoid spill over adjacent structures. Hence, it is unlikely that the entire CL was reached by injected viruses. Nevertheless, the partial inactivation of both CLs evoked a noticeable delay in the acquisition of CRs, without affecting URs. This delay in CR acquisition was evident not only in a qualitative sense (there were fewer CRs in early conditioning sessions; Fig. 8B), but also in a quantitative one (when CRs started appearing, they were considerably smaller; Fig. 8C–E). In contrast, we could not find any significant difference between the URs of blue and magenta groups; thus, CL shutdown affected the cognitive component of the task, but not the motor one. Furthermore, Chachich and Powell (2004) attained similar results—a delay in the acquisition of a classical heart rate conditioning—following permanent bilateral electrolytic lesion in the CL of rabbits. These results, together with the data illustrated in Figure 4, confirmed that CL neurons are not related to the kinematics of eyelid CRs, further support our previous statement about the CL being involved in the cognitive components of this type of associative learning.

In opposition to the role in the motor aspects of conditioned eyeblinks played by the cerebellum (Welsh and Harvey 1991; Krupa et al. 1993; Christian and Thompson 2003; Sánchez-Campusano et al. 2007; Ten Brinke et al. 2017) and the MC (Aou et al. 1992; Ammann et al. 2016), we believe that CL may be part of the several brain structures implicated in the cognitive component, mainly the hippocampus (Rescorla 1988; Múnera et al. 2001), CC (Weible et al. 2003; Hattori et al. 2014), and the mPFC (Powell et al. 2005; Leal-Campanario et al. 2007; Siegel and Mauk 2013; Caro-Martín et al. 2015).

The cognitive role of CL neurons could be related to the attentional process triggered by CS/US association, as reported by Goll et al. (2015). Furthermore, this putative role of the CL in the attentional and cognitive components of classical eyeblink conditioning has also been proposed for CL in other types of learning task, as a sort of resilience to distraction (Atlan et al. 2018). As shown here, reduction in claustral activities produces a noticeable deficit in the cognitive components of classical eyeblink conditioning. It has also been reported that CL presents a heightened activity in patients with attention deficit hyperactivity disorder as compared with controls

(Dickstein et al. 2006; Castellanos et al. 2008). Therefore, it is possible that a specific activation–inhibition balance of the CL cell population is needed to cope with complex cognitive challenges that require recruiting attention.

According to the present results, CL neurons are not activated by single and/or irrelevant stimuli of any sensory modality. In fact, they are activated by paired CS/US associations until the moment when CRs reach asymptotic values in their expression levels. In conclusion, the CL seems to play an important role in the proper acquisition of classical conditioning tasks, mostly in attentional processes related to CS/US association.

Supplementary Material

Supplementary material can be found at *Cerebral Cortex* online.

Funding

Notes

Authors' Contributions

Conception and design of the experiments: M.M.R.-G., A.G., J.M.D.-G. Performance of the experiments: M.M.R.-G., J.M.D.-G. Contribution of new analytic tools and representation programs: R.S.-C., J.L., G.K.D., M.T., M.T.H. Data analysis: M.M.R.-G., R.S.-C., J.M.D.-G. Preparation of the illustrations: M.M.R.-G., R.S.C., A.G. Drafting of the paper: M.M.R.-G., R.S.-C., A.G., J.M.D.-G. All authors revised the final version of the manuscript.

References

Ammann C, Márquez-Ruiz J, Gómez-Climent MÁ, Delgado-García JM, Gruart A. 2016. The motor cortex is involved in the generation of classically conditioned eyelid responses in behaving rabbits. *J Neurosci*. 36:6988–7001.

Aou S, Woody CD, Birt D. 1992. Changes in the activity of units of the cat motor cortex with rapid conditioning and extinction of a compound eyelid movement. *J Neurosci*. 12:549–559.

Atlan G, Terem A, Peretz-Rivlin N, Groysman M, Citri A. 2017. Mapping synaptic cortico-claustral connectivity in the mouse. *J Comp Neurol*. 525:1381–1402.

Atlan G, Terem A, Peretz-Rivlin N, Sehrawat K, Gonzales BJ, Pozner G, Tasaka GI, Goll Y, Refaeli R, Zviran O et al. 2018. The claustrum supports resilience to distraction. *Curr Biol*. 28:2752–2762.

Barthó P, Hirase H, Monconduit L, Zugaro M, Harris KD, Buzsáki G. 2004. Characterization of neocortical principal cells and interneurons by network interactions and extracellular features. *J Neurophysiol*. 92:600–608.

Berger TW, Rinaldi PC, Weisz DJ, Thompson RF. 1983. Single-unit analysis of different hippocampal cell types during classical conditioning of rabbit nictitating membrane response. *J Neurophysiol*. 50:1197–1219.

Bermudez-Rattoni F, Introini-Collison IB, McGaugh JL. 1991. Reversible inactivation of the insular cortex by tetrodotoxin produces retrograde and anterograde amnesia for inhibitory avoidance and spatial learning. *Proc Natl Acad Sci USA*. 88:5379–5382.

Blázquez PM, Fujii N, Kojima J, Graybiel AM. 2002. A network representation of response probability in the striatum. *Neuron*. 33:973–982.

Binks D, Watson C, Puelles L. 2019. A re-evaluation of the anatomy of the claustrum in rodents and primates—analyzing the effect of pallial expansion. *Front Neuroanat*. 13:34.

Bokil H, Andrews P, Kulkarni JE, Mehta S, Mitra PP. 2010. Chronux: a platform for analyzing neural signals. *J Neurosci Methods*. 192:146–151.

Buzsáki G, Kandel A. 1998. Somadendritic back propagation of action potentials in cortical pyramidal cells of the awake rat. *J Neurophysiol*. 79:1587–1591.

Carman JB, Cowan WM, Powell TP. 1964. The cortical projection upon the claustrum. *J Neurol Neurosurg Psychiatry*. 27:46–51.

Caro-Martín CR, Leal-Campanario R, Sánchez-Campusano R, Delgado-García JM, Gruart A. 2015. A variable oscillator underlies the measurement of time intervals in the rostral medial prefrontal cortex during classical eyeblink conditioning in rabbits. *J Neurosci*. 35:14809–14821.

Castellanos FX, Margulies DS, Kelly C, Uddin LQ, Ghaffari M, Kirsch A, Shaw D, Shehzad Z, Di Martino A, Biswal B et al. 2008. Cingulate-precuneus interactions: a new locus of dysfunction in adult attention-deficit/hyperactivity disorder. *Biol Psychiatry*. 63:332–337.

Cebolla AM, Cheron G. 2019. Understanding neural oscillations in the human brain: from movement to consciousness and vice versa. *Front Psychol*. 10:1930.

Chachich ME, Powell DA. 2004. The role of claustrum in Pavlovian heart rate conditioning in the rabbit (*Oryctolagus cuniculus*): anatomical, electrophysiological, and lesion studies. *Behav Neurosci*. 118:514–525.

Chia Z, Silberberg G, Augustine GJ. 2017. Functional properties, topological organization and sexual dimorphism of claustrum neurons projecting to anterior cingulate cortex. *Claustrum*. 2:1.

Chia Z, Augustine GJ, Silberberg G. 2020. Synaptic connectivity between the cortex and claustrum is organized into functional modules. *Curr Biol*. 30:2777–2790.

Christian KM, Thompson RF. 2003. Neural substrates of eyeblink conditioning: acquisition and retention. *Learn Mem*. 10:427–455.

Citri A, Barretta S. 2016. Claustral delusions. *Claustrum*. 1(1):31426.

Clark GA, McCormick DA, Lavond DG, Thompson RF. 1984. Effects of lesions of cerebellar nuclei on conditioned behav-

ioral and hippocampal neuronal responses. *Brain Res.* 291: 125–136.

Constantinidis C, Goldman-Rakic PS. 2002. Correlated discharges among putative pyramidal neurons and interneurons in the primate prefrontal cortex. *J Neurophysiol.* 88:3487–3497.

Crick FC. 1994. *The astonishing hypothesis.* New York (NY): Charles Scribner's Sons.

Crick FC, Koch C. 2005. What is the function of the claustrum? *Philos Trans R Soc Lond B Biol Sci.* 360:1271–1279.

Csicsvari J, Hirase H, Czurkó A, Mamiya A, Buzsáki G. 1999. Oscillatory coupling of hippocampal pyramidal cells and interneurons in the behaving rat. *J Neurosci.* 19:274–287.

Delgado-García JM, Evinger C, Escudero M, Baker R. 1990. Behavior of accessory abducens and abducens motoneurons during eye retraction and rotation in the alert cat. *J Neurophysiol.* 64:413–422.

Deligkaris K, Bullmann T, Frey U. 2016. Extracellularly recorded somatic and neuritic signal shapes and classification algorithms for high-density microelectrode array electrophysiology. *Front Neurosci.* 10:421. doi: 10.3389/fnins.2016.00421.

Dickstein SG, Bannon K, Castellanos FX, Milham MP. 2006. The neural correlates of attention deficit hyperactivity disorder: an ALE meta-analysis. *J Child Psychol Psychiatry.* 47:1051–1062.

Dogbevia GK, Roβmanith M, Sprengel R, Hasan MT. 2016. Flexible, AAV-equipped genetic modules for inducible control of gene expression in mammalian brain. *Mol Ther Nucleic Acids.* 5:e309.

Dogbevia GK, Marticorena-Alvarez R, Bausen M, Sprengel R, Hasan MT. 2015. Inducible and combinatorial gene manipulation in mouse brain. *Front Cell Neurosci.* 9:142.

Druga R. 1982. Claustro-neocortical connections in the cat and rat demonstrated by HRP tracing technique. *J Hirnforsch.* 23:191–202.

Druga R, Rokyta R, Benes V. 1990. Claustro-neocortical projections in the rhesus monkey (projections to area 6). *J Hirnforsch.* 31:487–494.

Duffau H, Mandonnet E, Gatignol P, Capelle L. 2007. Functional compensation of the claustrum: lessons from low-grade glioma surgery. *J Neurooncol.* 81:327–329.

Edelstein LR, Denaro FJ. 2004. The claustrum: a historical review of its anatomy, physiology, cytochemistry and functional significance. *Cell Mol Biol.* 50(6):675–702.

Fernández-Lamo I, Delgado-García JM, Gruart A. 2018. When and where learning is taking place: multisynaptic changes in strength during different behaviors related to the acquisition of an operant conditioning task by behaving rats. *Cereb Cortex.* 28:1011–1023.

Fernández-Lamo I, Sánchez-Campusano R, Gruart A, Delgado-García JM. 2016. Functional states of rat cortical circuits during the unpredictable availability of a reward-related cue. *Sci Rep.* 6:37650.

Gibbs CM, Prescott LB, Powell DA. 1992. A comparison of multiple-unit activity in the medial prefrontal and agranular insular cortices during Pavlovian heart rate conditioning in rabbits. *Exp Brain Res.* 89:599–610.

Girgis M, Shih-Chang W. 1981. *A new stereotaxic atlas of the rabbit brain.* St. Louis (MO): Warren H. Green, Inc.

Goll Y, Atlan G, Citri A. 2015. Attention: the claustrum. *Trends Neurosci.* 38:486–495.

Gruart A, Blázquez P, Delgado-García JM. 1995. Kinematics of spontaneous, reflex, and conditioned eyelid movements in the alert cat. *J Neurophysiol.* 74:226–248.

Gruart A, Muñoz MD, Delgado-García JM. 2006. Involvement of the CA3-CA1 synapse in the acquisition of associative learning in behaving mice. *J Neurosci.* 26:1077–1087.

Gruart A, Schreurs BG, del Toro ED, Delgado-García JM. 2000. Kinetic and frequency-domain properties of reflex and conditioned eyelid responses in the rabbit. *J Neurophysiol.* 83:836–852.

Hasan MT, Hernández-González S, Dogbevia G, Treviño M, Bertocchi I, Gruart A, Delgado-García JM. 2013. Role of motor cortex NMDA receptors in learning-dependent synaptic plasticity of behaving mice. *Nat Commun.* 4:2258.

Hattori S, Yoon T, Disterhoft JF, Weiss C. 2014. Functional reorganization of a prefrontal cortical network mediating consolidation of trace eyeblink conditioning. *J Neurosci.* 34:1432–1445.

Jackson J, Karnani MM, Zemelman BV, Burdakov D, Lee AK. 2018. Inhibitory control of prefrontal cortex by the claustrum. *Neuron.* 99:1029–1039.

Jankowski MM, Islam MN, O'Mara SM. 2017. Dynamics of spontaneous local field potentials in the anterior claustrum of freely moving rats. *Brain Res.* 1677:101–117.

Jurado-Parras MT, Sánchez-Campusano R, Castellanos NP, del-Pozo F, Gruart A, Delgado-García JM. 2013. Differential contribution of hippocampal circuits to appetitive and consummatory behaviors during operant conditioning of behaving mice. *J Neurosci.* 33:2293–2304.

Kowiański P, Dziewiątkowski J, Kowiańska J, Moryś J. 1999. Comparative anatomy of the claustrum in selected species: a morphometric analysis. *Brain Behav Evol.* 53:44–54.

Kowiański P, Moryś J, Dziewiatkowski J, Karwacki Z, Wisniewski HM. 2000. The combined retrograde transport and unbiased stereological study of the claustrocortical connections in the rabbit. *Ann Anat.* 182:111–122.

Kowiański P, Moryś J, Karwacki Z, Dziewiątkowski J, Narkiewicz O. 1997. The cortico-related zones of the rabbit claustrum— study of the claustrocortical connections based on the retrograde axonal transport of fluorescent tracers. *Brain Res.* 784:1–2.

Krupa DJ, Thompson JK, Thompson RF. 1993. Localization of a memory trace in the mammalian brain. *Science.* 260:989–991.

Kurada L, Bayat A, Joshi S, Koubeissi MZ. 2019. The claustrum in relation to seizures and electrical stimulation. *Front Neuroanat.* 13:8.

Leal-Campanario R, Delgado-García JM, Gruart A. 2013. The rostral medial prefrontal cortex regulates the expression of conditioned eyelid responses in behaving rabbits. *J Neurosci.* 33:4378–4386.

Leal-Campanario R, Fairén A, Delgado-García JM, Gruart A. 2007. Electrical stimulation of the rostral medial prefrontal cortex in rabbits inhibits the expression of conditioned eyelid responses but not their acquisition. *Proc Natl Acad Sci USA.* 104:11459–11464.

Lipski J. 1981. Antidromic activation of neurones as an analytic tool in the study of the central nervous system. *J Neurosci Methods.* 4:1–32.

Majak K, Kowiański P, Moryś J, Spodnik J, Karwacki Z, Wisniewski HM. 2000. The limbic zone of the rabbit and rat claustrum: a study of the claustrocingulate connections based on the retrograde axonal transport of fluorescent tracers. *Anat Embryol.* 201:15–25.

Marchi G, Bentivoglio M, Minciacchi D, Molinari M. 1983. Claustrocortical projections studied in the cat by means of multiple retrograde fluorescent tracing. *J Comp Neurol.* 215:121–134.

Masimore B, Kakalios J, Redish AD. 2004. Measuring fundamental frequencies in local field potentials. *J Neurosci Methods*. 138:97–105.

Mathur BN. 2014. The claustrum in review. *Front Syst Neurosci*. 8:48.

Minciacchi D, Molinari M, Bentivoglio M, Macchi G. 1985. The organization of the ipsi- and contralateral claustrocortical system in rat with notes on the bilateral claustrocortical projections in cat. *Neuroscience*. 16:557–576.

Mitra PP, Bokil H. 2008. *Observed brain dynamics*. New York (NY): Oxford University Press.

Múnera A, Gruart A, Muñoz MD, Fernández-Mas R, Delgado-García JM. 2001. Hippocampal pyramidal cell activity encodes conditioned stimulus predictive value during classical conditioning in alert cats. *J Neurophysiol*. 86:2571–2582.

Olson CR, Graybiel AM. 1980. Sensory maps in the claustrum of the cat. *Nature*. 288:479–481.

Oswald BB, Knuckley B, Mahan K, Sanders C, Powell DA. 2009. Prefrontal control of trace eyeblink conditioning in rabbits (Oryctolagus cuniculus) II: effects of type of unconditioned stimulus (airpuff vs. periorbital shock) and unconditioned stimulus intensity. *Physiol Behav*. 96:67–72.

Powell DA, Churchwell J, Burriss L. 2005. Medial prefrontal lesions and Pavlovian eyeblink and heart rate conditioning: effects of partial reinforcement on delay and trace conditioning in rabbits (Oryctolagus cuniculus). *Behav Neurosci*. 119:180–189.

Remedios R, Logothetis NK, Kayser C. 2009. An auditory region in the primate insular cortex responding preferentially to vocal communication sounds. *J Neurosci*. 29:1034–1045.

Remedios R, Logothetis NK, Kayser C. 2010. Unimodal responses prevail within the multisensory claustrum. *J Neurosci*. 30:12902–12907.

Remedios R, Logothetis NK, Kayser C. 2014. A role of the claustrum in auditory scene analysis by reflecting sensory change. *Front Syst Neurosci*. 8:44.

Rescorla RA. 1988. Behavioral studies of Pavlovian conditioning. *Annu Rev Neurosci*. 11:329–352.

Rieke F, Warland D, de Ruyter van Steveninck R, Bialek W. 1997. *Spikes: exploring the neural code*. Cambridge (MA): MIT Press.

Sánchez-Campusano R, Gruart A, Delgado-García JM. 2007. The cerebellar interpositus nucleus and the dynamic control of learned motor responses. *J Neurosci*. 27:6620–6632.

Schade Powers A, Coburn-Litvak P, Evinger C. 2010. Conditioned eyelid movement is not a blink. *J Neurophysiol*. 103:641–647.

Sherk H, LeVay S. 1981. Visual claustrum: topography and receptive field properties in the cat. *Science*. 212:87–89.

Siegel JJ, Mauk MD. 2013. Persistent activity in prefrontal cortex during trace eyelid conditioning: dissociating responses that reflect cerebellar output from those that do not. *J Neurosci*. 33:15272–15284.

Smith JB, Alloway KD. 2010. Functional specificity of claustrum connections in the rat: interhemispheric communication between specific parts of motor cortex. *J Neurosci*. 30:16832–16844.

Smith JB, Watson GDR, Liang Z, Liu Y, Zhang N, Alloway KD. 2019. A role for the claustrum in salience processing? *Front Neuroanat*. 13:64.

Smythies J, Edelstein L, Ramachandran V. 2012. Hypotheses relating to the function of the claustrum. *Front Integr Neurosci*. 6:53.

Spector I, Hassmannova J, Albe-Fessard D. 1974. Sensory properties of single neurons of cat's claustrum. *Brain Res*. 66:39–65.

Steriade M, Apostol V, Oakson G. 1971. Control of unitary activities in cerebellothalamic pathway during wakefulness and synchronized sleep. *J Neurophysiol*. 34:389–413.

Sweeney ST, Broadie K, Keane J, Niemann H, O'Kane CJ. 1995. Targeted expression of tetanus toxin light chain in Drosophila specifically eliminates synaptic transmission and causes behavioral defects. *Neuron*. 14:341–351.

Takehara-Nishiuchi K, Kawahara S, Kirino Y. 2005. NMDA receptor-dependent processes in the medial prefrontal cortex are important for acquisition and the early stage of consolidation during trace, but not delay eyeblink conditioning. *Learn Mem*. 12:606–614.

Ten Brinke MM, Heiney SA, Wang X, Proietti-Onori M, Boele HJ, Bakermans J, Medina JF, Gao Z, De Zeeuw CI. 2017. Dynamic modulation of activity in cerebellar nuclei neurons during pavlovian eyeblink conditioning in mice. *Elife*. 6:e28132.

Thompson RF. 2005. In search of memory traces. *Annu Rev Psychol*. 56:1–23.

Torgerson CM, Irimia A, Goh SY, Van Horn JD. 2015. The DTI connectivity of the human claustrum. *Hum Brain Mapp*. 36:827–838.

Viskontas IV, Ekstrom AD, Wilson CL, Fried I. 2007. Characterizing interneuron and pyramidal cells in the human medial temporal lobe in vivo using extracellular recordings. *Hippocampus*. 17:49–57.

Weible AP, Weiss C, Disterhoft JF. 2003. Activity profiles of single neurons in caudal anterior cingulate cortex during trace eyeblink conditioning in the rabbit. *J Neurophysiol*. 90:599–612.

Welsh JP, Harvey JA. 1991. Pavlovian conditioning in the rabbit during inactivation of the interpositus nucleus. *J Physiol (Lond)*. 444:459–480.

White MG, Cody PA, Bubser M, Wang HD, Deutch AY, Mathur BN. 2017. Cortical hierarchy governs rat claustrocortical circuit organization. *J Comp Neurol*. 525:1347–1362.

White MG, Panicker M, Mu C, Carter AM, Roberts BM, Dharmasri PA, Mathur BN. 2018. Anterior cingulate cortex input to the claustrum is required for top-down action control. *Cell Rep*. 22:84–95.